ACS Chemical Neuroscience

pubs.acs.org/chemneuro

Research Article

Sequestration of TDP-43$^{216-414}$ Aggregates by Cytoplasmic Expression of the proSAAS Chaperone

Juan R. Peinado,[#] Kriti Chaplot,[#] Timothy S. Jarvela, Edward M. Barbieri, James Shorter, and Iris Lindberg*

Cite This: https://doi.org/10.1021/acschemneuro.2c00156

Read Online

ACCESS | Metrics & More | Article Recommendations | Supporting Information

ABSTRACT: As neurons age, protein homeostasis becomes less efficient, resulting in misfolding and aggregation. Chaperone proteins perform vital functions in the maintenance of cellular proteostasis, and chaperone-based therapies that promote sequestration of toxic aggregates may prove useful in blocking the development of neurodegenerative disease. We previously demonstrated that proSAAS, a small secreted neuronal protein, exhibits potent chaperone activity against protein aggregation in vitro and blocks the cytotoxic effects of amyloid and synuclein oligomers in cell culture systems. We now examine whether cytoplasmic expression of proSAAS results in interactions with protein aggregates in this cellular compartment. We report that expression of proSAAS within the cytoplasm generates dense, membraneless 2 μm proSAAS spheres which progressively fuse to form larger spheres, suggesting liquid droplet-like properties. ProSAAS spheres selectively accumulate a C-terminally truncated fluorescently tagged form of TDP-43, initiating its cellular redistribution; these TDP-43-containing spheres also exhibit dynamic fusion. Efficient encapsulation of TDP-43 into proSAAS spheres is driven by its C-terminal prion-like domain; spheres must be formed for sequestration to occur. Three proSAAS sequences, a predicted coiled-coil, a conserved region (residues 158−169), and the positively charged sequence 181−185, are all required for proSAAS to form spheres able to encapsulate TDP-43 aggregates. Substitution of lysines for arginines in the 181−185 sequence results in nuclear translocation of proSAAS and encapsulation of nuclear-localized TDP-43$^{216-414}$. As a functional output, we demonstrate that proSAAS expression results in cytoprotection against full-length TDP-43 toxicity in yeast. We conclude that proSAAS can act as a functional holdase for TDP-43 via this phase-separation property, representing a cytoprotectant whose unusual biochemical properties can potentially be exploited in the design of therapeutic molecules.

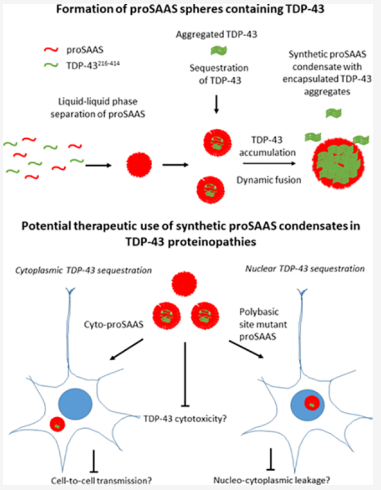

KEYWORDS: *proSAAS, PCSK1N, neurodegeneration, chaperone, TDP-43, neurodegeneration, proteostasis, liquid−liquid phase separation, ALS, FTD*

INTRODUCTION

In recent years, it has become increasingly apparent that many, if not all, neurodegenerative diseases involve the aggregation of key proteins, including Alzheimer's, Parkinson's, and Huntington's diseases as well as amyotrophic lateral sclerosis (ALS). During disease progression, misfolded proteins, with many containing intrinsically disordered domains, initiate a proteostatic cascade in which proteins are destabilized and precipitate, contributing to neurotoxic events that culminate in neuronal death.[1,2] Examples of cytoplasmic aggregates involved in neuropathology include aggregated alpha-synuclein (α-Syn), the major component of the cellular hallmark of Parkinson's disease, Lewy bodies, and the RNA-binding protein TAR DNA binding domain protein 43 (TDP-43), which normally shuttles between the cytoplasm and nucleus but is mislocalized to cytoplasmic aggregates in more than 95% of patients with ALS and in 45% of those with frontotemporal lobar dementia (FTLD) (refs 3 and 4; reviewed in ref 5). TDP-43 is post-translationally modified by phosphorylation and ubiquitination as well as by cleavage of its aggregation-prone carboxy-terminal prion-like domain; all of these modifications are strongly implicated in disease pathology.[4] These abnormal proteins undergo liquid−liquid phase separation (LLPS) to form liquid condensates en route to the formation of solid phase aggregates (e.g., ref 6). LLPS is thought to be important to proteostatic control during cellular stress.[7]

Increasing evidence points to important roles for cellular and secreted chaperones in the formation and deposition of abnormal protein aggregates in neurodegenerative disease

Received: March 9, 2022
Accepted: April 20, 2022

(reviewed in refs 2 8,−910). Chaperone proteins may act to sequester misfolded proteins, refold unfolded proteins, and cooperate with degradative machinery, either directly or indirectly, to facilitate the degradation of misfolded species and/or enhance disaggregation (see the above reviews). Overexpression of cytoplasmic chaperones mitigates aggregate toxicity,[2,11,12] whereas overexpression of the constitutively secreted secretory chaperones clusterin and α2-macroglobulin is neuroprotective in Neuro2A cells,[13] reviewed in ref 14.

Despite the enhanced susceptibility of neurons to proteostatic disease, few neuron-specific chaperones have been identified in brain tissues. We have previously reported that the neuronally expressed secretory chaperone proSAAS (gene name: *PCSK1N*) potently blocks the fibrillation of neurodegenerative disease-related proteins such as β-amyloid and α-Syn and is cytoprotective against oligomers of these two proteins.[15,16] ProSAAS immunoreactivity colocalizes with inclusion bodies in a variety of neurodegenerative diseases,[15−18] supporting a role for proSAAS in disease control. Interestingly, 10 independent proteomics studies have identified proSAAS as a differentially expressed biomarker in the cerebrospinal fluid obtained from dementia patients.[19−28] Recent transcriptomics studies of Alzheimer's brain tissue show that proSAAS expression increases during disease progression,[29] and other studies indicate that proSAAS synthesis is highly increased in a hippocampal model of homeostatic scaling.[30]

These data implicating proSAAS in neurodegenerative disease have prompted us to investigate a potential role for the proSAAS chaperone in handling misfolded proteins involved in neurodegeneration-related processes in living cells. Unexpectedly, we found that cytoplasmic expression of proSAAS results in the formation of unique spherical structures that exhibit a great affinity for TDP-43 aggregates. We suggest that these synthetic spherical structures present an opportunity for therapeutic entrapment of toxic TDP-43 aggregates.

RESULTS

To explore the role of proSAAS as a chaperone in neurodegenerative diseases, we performed cell culture-based coexpression studies to identify potential client proteins that are prone to aggregation. We first expressed secreted FLAG-tagged proSAAS ("sec-proSAAS", Figure 1A), which naturally localizes to the secretory pathway of HEK and Neuro2A cells, but since many aggregating proteins involved in neurodegeneration are cytoplasmic, we also expressed a FLAG-tagged proSAAS construct lacking a signal peptide ("cyto-proSAAS"; Figure 1A).

Cytoplasmic Expression of proSAAS Results in the Formation of Dense Antibody-Impenetrable Spherical Structures that Specifically Encapsulate GFP-TDP-43$^{216-414}$ Aggregates. Following transfection of sec-proSAAS into Neuro2A cells and staining with the FLAG antibody, we observed proSAAS staining in puncta and small spheres (Figure 1A). In sec-proSAAS-expressing HEK cells, proSAAS staining presented as much larger (1 μm) spherical structures, likely within the secretory pathway (Figure 1A). Expression of the cyto-proSAAS construct in both HEK (Figure 1B) and Neuro2A cells (Figure S1A) resulted in the appearance of large FLAG-immunoreactive spherical structures in the cytosol. In Neuro2A cells, these spheres exhibited an average size of 2 ± 1 μm. Similar results were found in HEK cells at 24 h after transfection, although the size of the spheres was greater, with an average diameter of 4 ± 2 μm. This pattern of expression remained constant at 48 h in Neuro2A cells (Figure S1A), but in HEK cells, the size of the spheres increased at this time point, suggesting increased proSAAS recruitment (Figure 1B). ProSAAS spheres were easily observable at 40× using phase-contrast microscopy (Figure S1B). Western blotting of cyto-proSAAS-transfected HEK cells revealed the expected band of approximately 30 kDa, corresponding to full-length proSAAS (Figure S1B). Transfected hippocampal neurons also exhibited cyto-proSAAS spheres (Figure S1C), suggesting that proSAAS sphere formation is not restricted to propagating cell lines.

We then performed stimulated emission depletion (STED) imaging of the sec-proSAAS sphere morphology, which confirmed the presence of 1 μm-sized spheres stained with the FLAG antibody within the secretory pathway (Figure 1C). Similar experiments performed with cyto-proSAAS revealed the presence of an undulated surface on 2−4 μm large spheres (Figure 1C). Taken together, these data show that the proSAAS chaperone is not diffusely expressed within either the secretory pathway or the cytoplasm but instead strongly self-associates, condensing into distinct spheres.

To investigate how proSAAS forms these spherical assemblies, we attached an amino-terminal mCherry tag to the cyto-proSAAS construct ("mCherry-cyto-proSAAS") and transfected this construct into Neuro2A cells. Surprisingly, rather than forming spheres, mCherry-cyto-proSAAS formed dispersed aggregates throughout the cytosol, indicating possible misfolding (Figure S1D). Reducing the concentration of mCherry-cyto-proSAAS cDNA by dilution with a sixfold excess of non-mCherry-tagged cyto-proSAAS cDNA resulted in the formation of dense cyto-proSAAS spheres which were uniformly labelled with mCherry fluorescence (Figure 1D). We surmise that excess cyto-proSAAS interacts with mCherry-cyto-proSAAS, enabling sphere formation.

To identify potential aggregating client proteins for the cyto-proSAAS chaperone, we expressed cyto-proSAAS together with cDNAs encoding various GFP-tagged cytoplasmic proteins implicated in neurodegenerative diseases and known to aggregate intracellularly, including synuclein, tau, huntingtin polyQ repeats (HTT-Q74), and TDP-43.[31−34] GFP-tagged synuclein and tau and their respective mutants synuclein A53T and TauE14 exhibited uniform cytoplasmic distribution, while HA-tagged and GFP-tagged HTT-Q74 and the TDP-43 C-terminal construct GFP-TDP-43$^{216-414}$ formed dispersed cytoplasmic inclusions when expressed alone in HEK cells (Figure S1E). While these non-aggregating forms of synuclein and tau failed to interact with cyto-proSAAS spheres, the distribution of GFP-TDP-43$^{216-414}$ aggregates was profoundly altered by coexpression of cyto-proSAAS, becoming localized predominantly within the proSAAS sphere cores. This occurred in both Neuro2A (Figure 1E, upper row) and HEK cells (Figure S2B). In contrast, neither HA-tagged HTT-Q74 nor GFP-HTT-Q74 aggregates were incorporated into spheres (Figure S2C,D), nor was mCherry incorporated (Figure 1E, lower row; S2E). Cytoplasmic GFP-TDP-43$^{216-414}$ located outside cyto-proSAAS spheres, but not encapsulated GFP-TDP-43$^{216-414}$, could be visualized using TDP-43 antibody staining, supporting the idea that cyto-proSAAS spheres are antibody-impenetrable (Figure 1F). These data indicate that this aggregation-prone[31] TDP-43 C-terminal protein exhibits a great affinity for the interior of the proSAAS sphere.

We then used transmission electron microscopy to gain a better structural understanding of the proSAAS-TDP-43$^{216-414}$ sphere structure (Figure 2A). When transfected alone, GFP-TDP-43$^{216-414}$ accumulated in small amorphous aggregates of

https://doi.org/10.1021/acschemneuro.2c00156
ACS Chem. Neurosci. XXXX, XXX, XXX−XXX

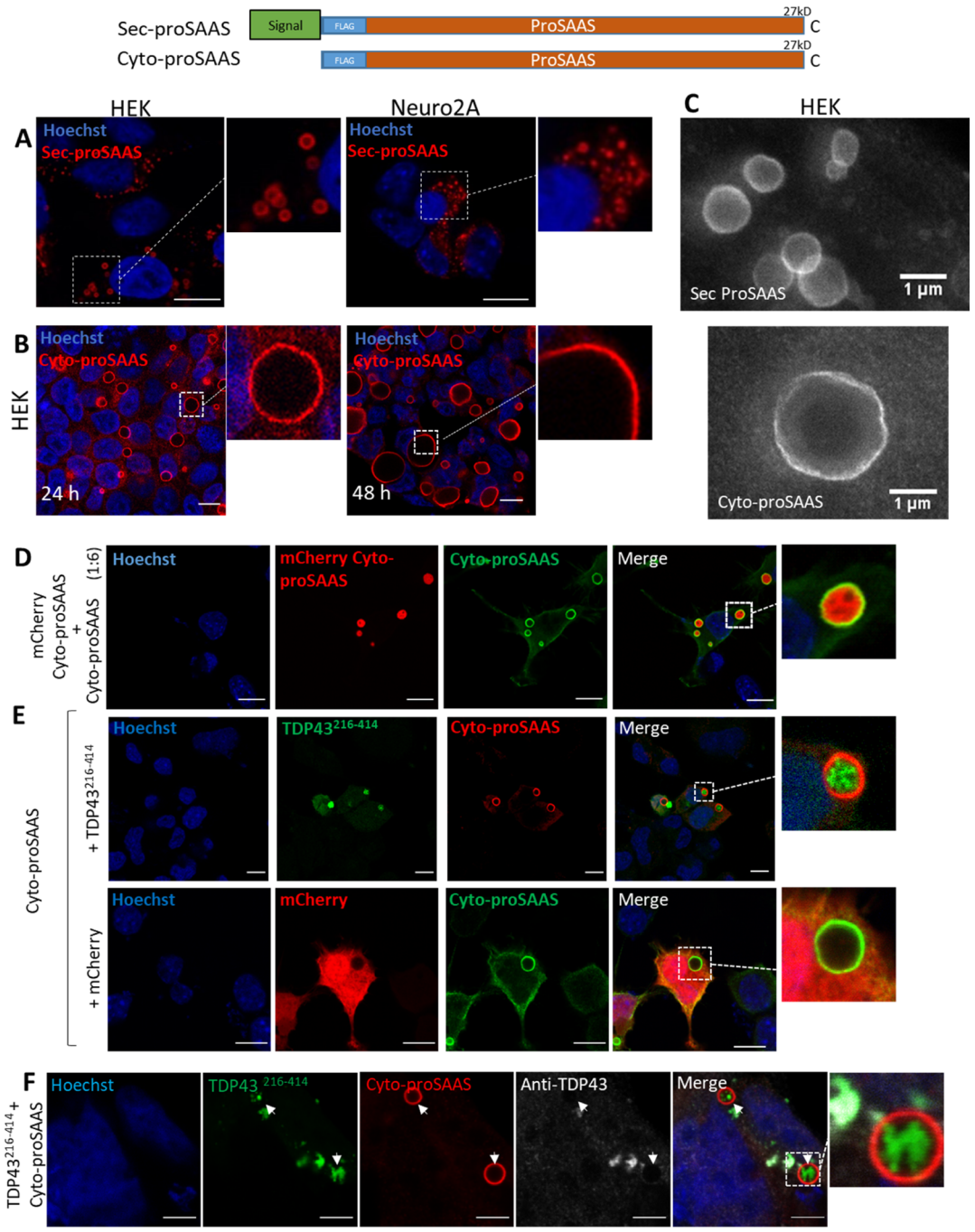

Figure 1. Cytoplasmic expression of proSAAS leads to the formation of dense antibody-impenetrable spheres that specifically encapsulate TDP-43$^{216-414}$ aggregates. Constructs used are shown above the figure, with the FLAG tag shown in blue and the signal peptide in green. (A) Immunostaining of secretory proSAAS (sec-proSAAS) expressed for 48 h (red) reveals the appearance of spheres in HEK cells (left). Neuro2A cells rarely exhibit annulated spheres (right). (B) Representative confocal images of HEK cells transfected with cyto-proSAAS cDNA. 48 h after transfection, the spheres are larger in size than at 24 h (left vs right sides). (C) Representative STED images of FLAG-immunoreactive spheres formed by overexpressed secretory proSAAS (top) and cyto-proSAAS (bottom) in HEK cells. (D) Cotransfection of small amounts of mCherry-cyto-proSAAS with a large (sixfold) excess of cyto-proSAAS (green) results in dense fluorescent mCherry-tagged proSAAS spheres. (E) (top row) TDP-43$^{216-414}$ aggregates are found inside cyto-proSAAS spheres (red) when both are coexpressed in Neuro2A cells. (E) (bottom row) Characteristic cytosolic fluorescence of the control protein mCherry (red), which is not accumulated within cyto-proSAAS spheres (green) when both are coexpressed in Neuro2A cells. (F) Lack of immunostaining of Neuro2A cells with the GFP-TDP-43 antibody (C-terminal; in white) after coexpression of cyto-proSAAS (red) and TDP-43$^{216-414}$ (green) shows that this antibody cannot penetrate the sphere, supporting core inaccessibility. The arrow indicates fluorescent but immunologically undetectable TDP-43$^{216-414}$ aggregates inside spheres. Images taken at 40×, 24 h after transfection. Scale bar, 10 μm. Magnified insets correspond to 10 μm.

100−500 nm (Figure 2A, top). Cells transfected with both cyto-proSAAS and GFP-TDP-43$^{216-414}$ cDNA contained electron-dense spheres of the expected size, in agreement with immunofluorescence experiments (Figure 2A, bottom; Figure 2B). The uniform electron density of these spheres did not reflect the polydispersity of internal GFP-TDP-43$^{216-414}$

https://doi.org/10.1021/acschemneuro.2c00156
ACS Chem. Neurosci. XXXX, XXX, XXX−XXX

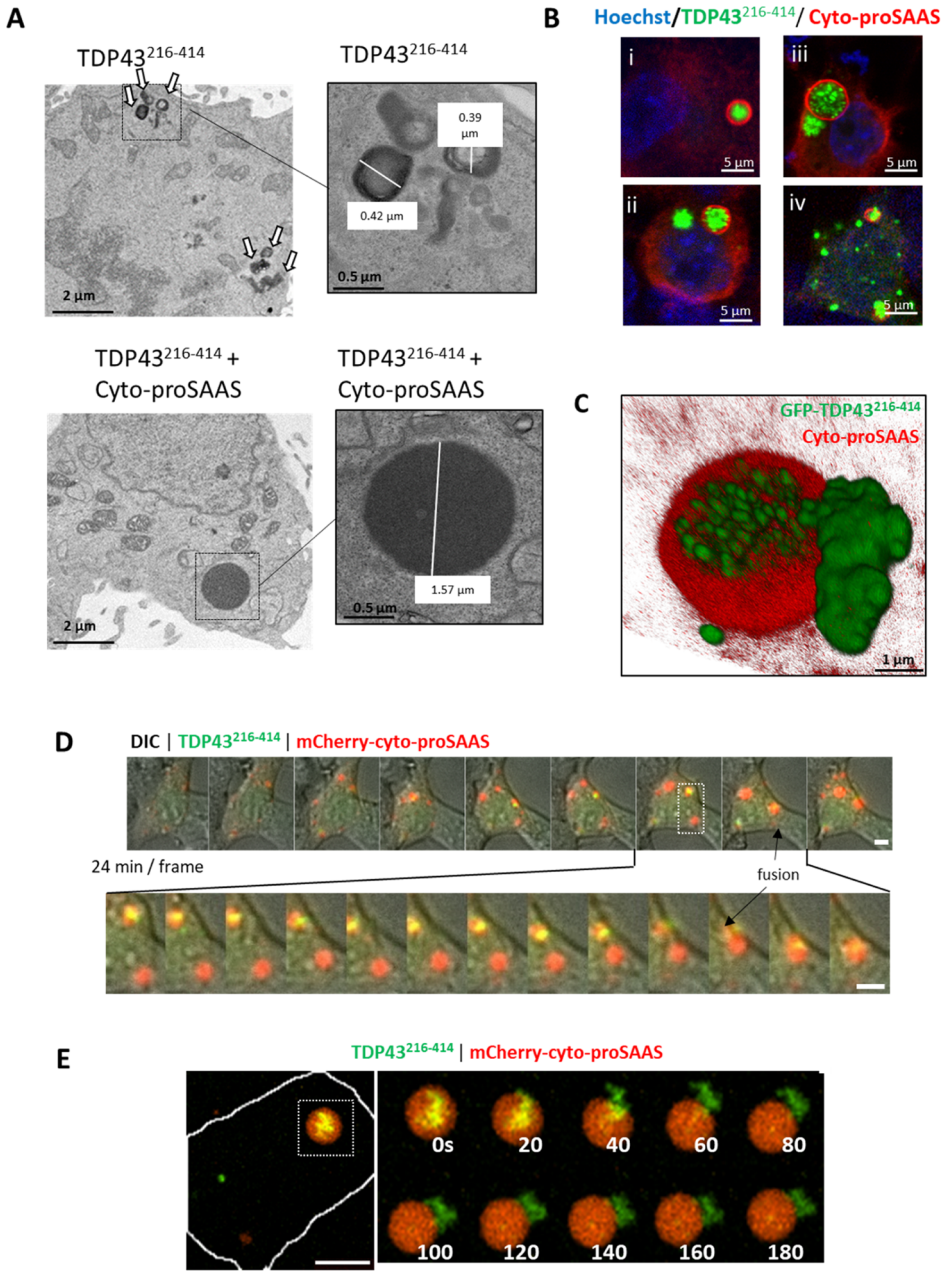

Figure 2. Cyto-proSAAS spheres are electron-dense and display simultaneous dynamic fusion and encapsulation of GFP-TDP-43$^{216-414}$ aggregates. (A) (top) Electron microscopy images of HEK cells transfected only with GFP-TDP-43$^{216-414}$. The characteristic GFP-TDP-43$^{216-414}$ aggregates are indicated with arrows, and a magnified image is shown at right. (A) (bottom) Electron microscopy images of HEK cells expressing GFP-TDP-43$^{216-414}$ and cyto-proSAAS, showing the characteristic dense spheres. (B) Confocal microscopy images of HEK cells cotransfected with GFP-TDP-43$^{216-414}$ and cyto-proSAAS cDNAs showing differing TDP-43 morphologies. Red, cyto-proSAAS; green, GFP-TDP-43$^{216-414}$. (C) 3D visualization of the spherical cyto-proSAAS-TDP-43$^{216-414}$ assembly. Red, cyto-proSAAS; green, GFP-TDP-43$^{216-414}$. (D,E) Dynamic widefield microscopy of mCherry-cyto-proSAAS (red) and GFP-TDP-43$^{216-414}$ (green, with DIC) beginning 18 h post transfection, taken at 2 min intervals for 5 h. See also Supporting Information Movies 1 and 2. (D) Images, taken at 24 min intervals (top), depict the generation of multiple spheres, with some containing GFP-TDP-43$^{216-414}$ aggregates which condense and fuse into larger spheres. A subset of images (box) is shown below at 2 min intervals, which captures two large spheres condensing into one. Scale bar, 10 μm. Magnified inserts correspond to 10 μm. (E) Rarely, internal GFP-TDP-43$^{216-414}$ was observed to rapidly and wholly exit from the center of cyto-proSAAS spheres. Max projections are shown, but a 3D analysis reveals GFP-TDP-43$^{216-424}$ to be contained entirely within the sphere at the beginning of the time course. Cyto-proSAAS, GFP-TDP-43$^{216-414}$, and mCherry-cyto-proSAAS were cotransfected in a ratio 1:1:0.2, as indicated in the Experimental Procedures section. Scale bar, 10 μm. Magnified inserts correspond to 10 μm.

aggregates seen in fluorescence images. These electron density data indicate that cyto-proSAAS spheres are not hollow but contain encapsulated material including cyto-proSAAS and TDP-43$^{216-414}$. This conclusion is supported by a 3D-rendered image which clearly shows immunoreactive proSAAS surrounding internalized GFP-TDP-43$^{216-414}$ (Figure 2C).

Dynamic Fusion of Liquid-like Cyto-proSAAS Spheres Containing GFP-TDP-43$^{216-414}$ Aggregates Indicates Properties Consistent with Phase Separation. To view the dynamics of cyto-proSAAS sphere formation, we performed widefield microscopy beginning 18 h after triple transfection of HEK cells with cDNAs encoding cyto-proSAAS, GFP-TDP-

https://doi.org/10.1021/acschemneuro.2c00156
ACS Chem. Neurosci. XXXX, XXX, XXX−XXX

$43^{216-414}$, and mCherry-cyto-proSAAS (in the weight ratio of 1:1:0.2; see the Experimental Procedures section). Cyto-proSAAS spheres first formed as several smaller spheres before fusing into only one or a few large spheres per cell, demonstrating LLPS-like ability (Figure 2D; see also Supporting Information Movie 1, cyto-proSAAS alone, and Supporting Information Movie 2, cyto-proSAAS with GFP-TDP-$43^{216-414}$). Small spheres also took up GFP-TDP-$43^{216-414}$ aggregates while continuing to fuse further. Occasionally, but only rarely, we observed full extrusion of GFP-TDP-$43^{216-414}$ aggregates from the center of cyto-proSAAS spheres (Figure 2E). When this occurred, the entirety of the GFP-TDP-$43^{216-414}$ content was removed over the course of 40 s, showing that encapsulation is a reversible process. However, since most cellular GFP-TDP-$43^{216-414}$ was encapsulated, extrusion is likely energetically less probable than uptake. Taken together, these data support fluidic properties of TDP-43-containing spheres.

Cyto-proSAAS Spheres Do Not Contain Markers Corresponding to Known Organelles. Cyto-proSAAS spheres appear to represent an unusual cytoplasmic structure. To gain information as to whether cyto-proSAAS spheres possess markers corresponding to known organelles or fuse with known organelles, we stained sphere surfaces with antisera directed against various cellular markers characteristic of different organelles. LC3-mCherry, an autophagosomal marker, did not colocalize or become sequestered by cyto-proSAAS, indicating that cyto-proSAAS sphere formation does not pertain to autophagic degradation (Figure S3A). Markers of lysosomes (Lamp-1, Lysotracker, Figure S3B,C), Golgi (giantin, Figure S3D), and lipid droplets (Bodipy, Figure S3E) also failed to stain cyto-proSAAS spheres. Antisera against HSP70 showed cytosolic labeling not associated with spheres (Figure S3F). The stress granule marker GFP-G3BP1 neither colocalized with nor became encapsulated by cyto-proSAAS (Figure S3G). Collectively, these data support the idea that cyto-proSAAS forms membraneless condensates in the cytosol.

Cyto-proSAAS Expression Assists the Accumulation of TDP-$43^{216-414}$ Aggregates. Since cyto-proSAAS efficiently captured GFP-TDP-$43^{216-414}$ aggregates, we examined the effect of cyto-proSAAS on the kinetics of TDP-43 degradation. We used cycloheximide to disrupt protein synthesis during a 6 h period following cotransfection of GFP-TDP-$43^{216-414}$ with cyto-proSAAS. Western blotting was employed to examine the level of cellular GFP-TDP-$43^{216-414}$ forms over time. Interestingly, the half-life of intact GFP-TDP-$43^{216-414}$ was significantly increased upon coexpression of cyto-proSAAS (Figure S4A). More than 80% of the GFP-TDP-$43^{216-414}$ protein was degraded after 6 h, whereas 43% of this protein was still present following coexpression with cyto-proSAAS at this time point. Figure S4A,B shows representative confocal microscopy images of HEK cells expressing GFP-TDP-$43^{216-414}$ with or without cyto-proSAAS and/or cycloheximide treatment, showing the cellular persistence of GFP-TDP-$43^{216-414}$ sequestered inside cyto-proSAAS spheres following cycloheximide treatment.

To obtain quantitative and qualitative comparisons of the characteristics of GFP-TDP-$43^{216-414}$ aggregates in the core versus the exterior of the proSAAS spheres, we analyzed Z-stacks of these cells (Figure S4C–E). We observed that the surface area to volume ratio of GFP-TDP-$43^{216-414}$ aggregates found inside the spheres was significantly larger (i.e., more loosely packed/dispersed) than that of aggregates found outside the spheres (Figure S4C). We also noted that the internal GFP-TDP-$43^{216-414}$ fluorescence, described as both mean pixel intensity (Figure S4D) and total signal intensity (Figure S4E), was significantly lower than that found in aggregates surrounding the spheres. We interpret this reduced compactness as possible evidence that GFP-TDP-$43^{216-414}$ aggregates are remodeled within the sphere core by interactions with internal cyto-proSAAS molecules.

Truncated Cytoplasmic TDP-43 C-Terminal Constructs Enter Cyto-proSAAS Sphere Cores. To identify the specific region of TDP-43 responsible for its entry into cyto-proSAAS spheres, we overexpressed five TDP-43 constructs tagged C-terminally with GFP together with cyto-proSAAS, each consisting of different protein domains (see the scheme in Figure 3A).[31] Similar to published studies,[31] the C-terminal constructs TDP-$43^{216-414}$ (as in Figure S1E), TDP-43^{86-414} (Figure 3B), and TDP-$43^{170-414}$ (Figure 3C) formed cytosolic aggregates by themselves, whereas TDP-$43^{257-414}$ (Figure 3D) was diffusely expressed in the cytosol. The C-terminal TDP-43 constructs TDP-$43^{216-414}$, TDP-43^{86-414}, and TDP-$43^{170-414}$ contain the prion-like domain and the RNA-binding domain harboring a nuclear export signal,[31] while the shorter, non-aggregating TDP-$43^{257-414}$ protein (Figure 3A) contains only the prion-like domain. Upon coexpression with cyto-proSAAS, all four of these C-terminal constructs were efficiently recruited into cyto-proSAAS spheres, indicating that it is the prion-like domain, and not the RNA-binding domain, that underlies the affinity of TDP-43 for cyto-proSAAS. In contrast, the N-terminal domain constructs GFP-TDP-43^{1-193} and GFP-TDP-43^{1-274} were concentrated within the nucleus, did not form aggregates, and were not recruited to cyto-proSAAS spheres (Figure S5).

The lack of full-length TDP-43 expression in the cytoplasm made it impossible to determine the contribution of the N-terminal regions of TDP-43 to proSAAS interactions. To circumvent this, we obtained HEK cells that inducibly express either wild-type full-length TDP-43 (TDP-43^{wt}) or full-length TDP-43 lacking NLS (TDP-$43^{\Delta NLS}$), both tagged N-terminally with GFP.[35] After 24 h of doxycycline exposure, we found that wild-type TDP-43 was localized to the nucleus, whereas the NLS-lacking mutant was present in the cytosol. To test for possible TDP-43 encapsulation, we transfected cells with cyto-proSAAS cDNA for 24 h and then induced cells with doxycycline for another 24 h to permit TDP-43 expression (see the scheme in Figure 3E). While nuclear TDP-43^{wt} was not sequestered by cytoplasmic proSAAS spheres due to the lack of colocalization (Figure 3E, top), the cytoplasmic TDP-$43^{\Delta NLS}$ mutant was efficiently encapsulated (Figure 3E, bottom).

Taken together, these results indicate that TDP-43 encapsulation by proSAAS is driven by the C-terminal prion-like domain.

Structural Requirements for Efficient Cyto-proSAAS Sphere Formation and TDP-$43^{216-414}$ Sequestration. To understand the structural requirements for proSAAS sphere formation, we performed structure–function experiments using deletion and mutation constructs. ProSAAS is rich in relatively hydrophobic amino acids such as alanine (18.7%) and proline (14.7%) as well as the positively charged amino acids arginine (13.8%) and lysine (12.4%). ProSAAS also contains several low-complexity regions (LCRs) and intrinsically disordered domains (IDDs) distributed throughout the length of the protein, as identified by PLAtform of TOols for LOw Complexity using the SEG tool[36] and the Predictor of Natural Disordered Regions tool, respectively (Figure S6).

Based on these predictions, we generated a variety of FLAG-tagged cyto-proSAAS constructs lacking specific segments of

https://doi.org/10.1021/acschemneuro.2c00156
ACS Chem. Neurosci. XXXX, XXX, XXX–XXX

Table 1. Summary of Properties of Cyto-proSAAS Deletion and Mutant Constructs[a]

construct	sphere formation (cyto-proSAAS alone)	fold change in diffuse proSAAS cytoplasmic intensity	fold change in the number of transfected cells with puncta/aggregates	TDP-43 sequestration
cyto-proSAAS	yes	1.0[b]	1.0[b]	yes
Δ1−30	yes	0.6×	11× puncta	yes
Δ37−70	yes	2.6×	no puncta or aggregates (only spheres and diffuse)	no
Δ78−98	yes (∼35% smaller)	0.6×	2× puncta	yes
Δ113−134	yes	1.4×	3.4× puncta	yes
Δ158−169	no	4×	11× puncta/7× aggregates	no
Δ163−185	no	3.3×	no puncta or aggregates (only diffuse)	no
Δ181−225	no	1.5×	1.8× puncta	no
Δ181−185	no	1.3×	5× puncta/30× aggregates	no
Δ190−225	yes	0.6×	10× puncta	yes
polybasic site mutant	yes (nuclear)	1.0	no puncta or aggregates (only spheres)	yes (nuclear)

[a]Punctal size: <1 μm^2; aggregate size: >1 μm^2. [b]Normalized baseline.

amino acids within the IDDs and LCRs: 1−30, 37−70, 78−98, 113−134, 163−185, 181−225, and 190−225 (Figures 4A and S6A). Constructs that retained the ability to form spheres exhibited either punctate (Δ1−30, Δ113−134, Δ190−225) or diffuse (Δ37−70, Δ113−134) immunoreactivity, suggesting different types of cytoplasmic assemblies (Figure 4A; summarized in Table 1). Most importantly, we found that the loss of segments 163−185 and 181−225 completely abolished the ability of proSAAS to form spheres (Figure 4A; Table 1), whereas the loss of residues 190−225 did not. Taken together, these data support the idea that proSAAS residues 163−189, containing a portion of the conserved region 158−169,[16] as well as the highly positively charged Arg^{181}-Arg-Leu-Arg-Arg^{185} sequence strongly contribute to the intermolecular and/or intramolecular interactions that enable sphere assembly.

To further test the contribution of these specific sequences, we deleted and/or mutated them and tested the resulting constructs' ability to generate spheres after transfection. We observed that transfection of constructs lacking the conserved residues 158−169 did not result in sphere formation but showed a diffuse morphology with occasional aggregates, thus supporting the importance of this sequence in cyto-proSAAS self-assembly (Figure 4A, Δ158−169, panel 9; Table 1).

Interestingly, deletion of the polybasic region resulted in massive impairment in the phase separation ability of cyto-proSAAS, observed as a change to diffuse cytoplasmic localization accompanied by highly intense asymmetric aggregates (Figure 4A, Δ181−185, panel 10; Table 1). In contrast, mutating the four arginines within this polybasic site to lysines, thereby conserving positive charge, resulted in the apparent creation of a nuclear import signal such that proSAAS spheres now formed within the nucleus (Figure 4A, polybasic site mutant, panel 11; Table 1). These results clearly demonstrate that positively charged amino acids within the 181−185 region are required for cyto-proSAAS sphere formation. We conclude that both the stretch of amino acids encompassing the conserved region 158−169 and the positively charged 181−185 segment are critical to proSAAS sphere assembly.

Our next goal was to assess whether these same mutated cyto-proSAAS constructs could also sequester GFP-TDP-$43^{216-414}$. We found that most constructs that retained the ability to form spheres were also able to successfully encapsulate GFP-TDP-$43^{216-414}$ (Figure 4B, Table 1). One exception was the cyto-proSAAS Δ37−70 construct. When expressed alone, this construct showed diffuse staining but efficiently formed spheres, but when coexpressed with GFP-TDP-$43^{216-414}$, it both failed to form spheres and was unable to encapsulate GFP-TDP-$43^{216-414}$ (Figure 4B, 37−70, panel 3; Table 1). GFP-TDP-$43^{216-414}$ fluorescence expressed in the presence of this construct also appeared diffuse rather than punctate. According to the recent AlphaFold simulated structure (https://alphafold.ebi.ac.uk/entry/Q9QXV0) and DeepMind predictions (https://toolkit.tuebingen.mpg.de/tools/deepcoil), residues 37−70 in proSAAS are contained within a strongly predicted coiled-coil (residues 32−80); this region appears to be involved in TDP-43 interactions.

In contrast, the cyto-proSAAS Δ113−134 construct, which exhibited both punctate and diffuse localization, still retained the ability both to form spheres and to sequester GFP-TDP-$43^{216-414}$ (Figure 4B, 113−134, panel 5; Table 1). Cyto-proSAAS constructs lacking either the 158−169 conserved region (Figure 4B, 163−185, panel 6; 158−169, panel 9) or the polybasic site (Figure 4B, 163−185, panel 6; 181−225, panel 7; 181−185, panel 10; Table 1) did not form spheres in GFP-TDP-$43^{216-414}$ coexpression experiments and hence did not sequester GFP-TDP-$43^{216-414}$. Interestingly, polybasic site mutation of arginines to lysines resulted in the redistribution of proSAAS spheres to the nucleus, and coexpression of GFP-TDP-$43^{216-414}$ resulted in nuclear-localized proSAAS spheres containing this protein (Figure 4B, panel 11; Table 1). These data support the idea that it is the C-terminal prion-like domain of TDP-43 which underlies the affinity of TDP-43 for proSAAS spheres, both within the cytoplasm and inside the nucleus.

In summary, this proSAAS-TDP-43 encapsulation structure−function analysis shows that the N-terminal 30 residues, the middle 78−98 residues, and the C-terminal 190−225 residues of proSAAS are completely dispensible for GFP-TDP-$43^{216-414}$ sequestration, whereas residues 37−70 and 158−189 are absolutely required. Importantly, these data also indicate that sphere formation is required for TDP-43 sequestration.

The above data strongly suggest that proSAAS and TDP-43 interact. To determine whether proSAAS can impact TDP-43 aggregation kinetics, we used a previously published assay and available constructs[16,37] to purify a TDP-43 analogue and recombinant proSAAS from bacteria (Figure S7A,B) and perform in vitro aggregation assays with TDP-43 and either recombinant proSAAS or the control protein bovine serum albumin (BSA). This TDP-43-His-MBP construct[37] contains a tobacco etch virus (TEV) protease cleavage site between TDP-

https://doi.org/10.1021/acschemneuro.2c00156
ACS Chem. Neurosci. XXXX, XXX, XXX−XXX

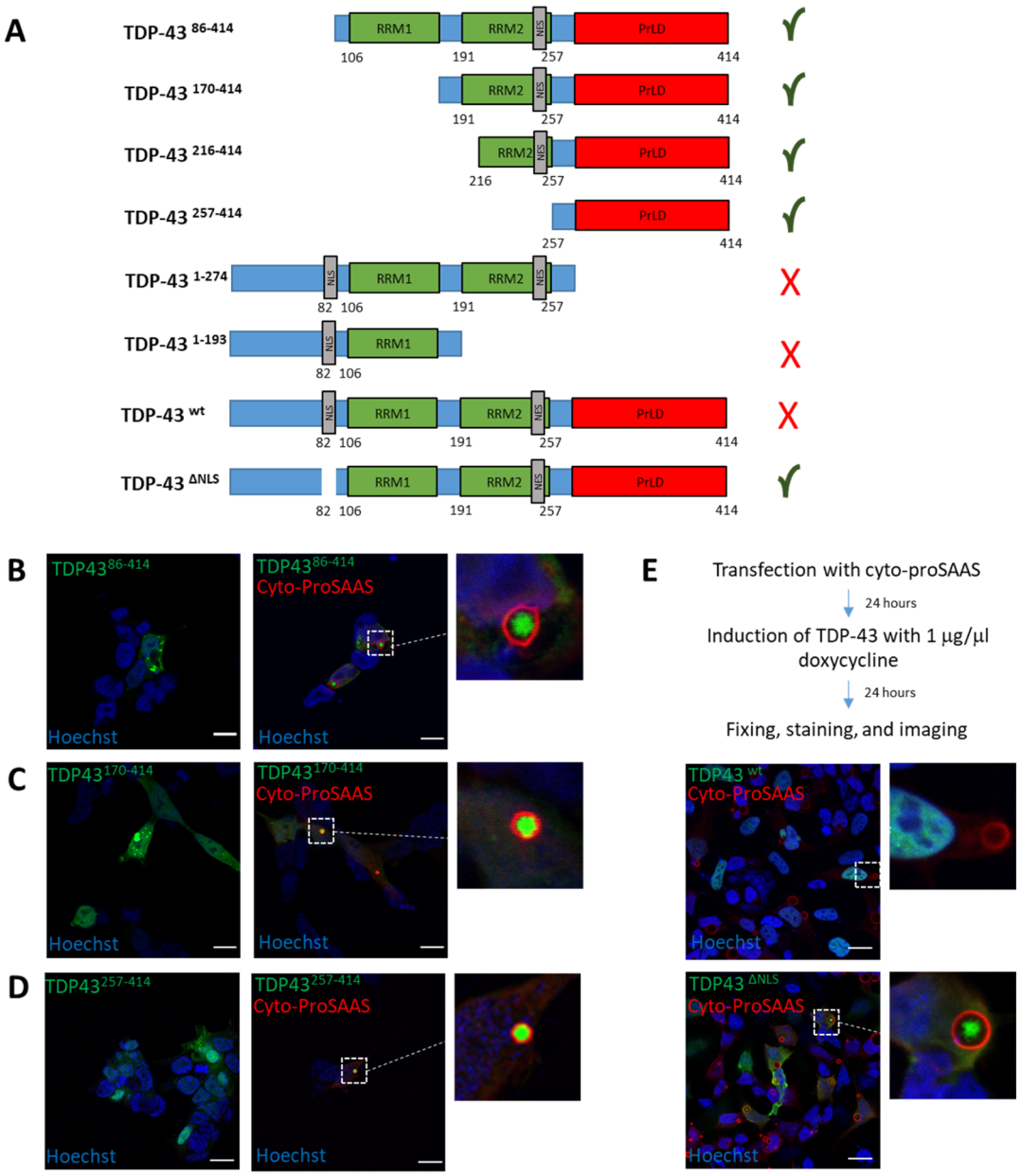

Figure 3. Cytoplasmic TDP-43 constructs containing the prion-like domain are sequestered by cyto-proSAAS spheres. (A) Schematic view of TDP-43 constructs; the C-terminal GFP tag is not shown. Red Xs indicate the lack of proSAAS encapsulation. (B,C) GFP-TDP-43$^{86\text{-}414}$(B) and GFP-TDP-43$^{170\text{-}414}$ (C) formed aggregates when expressed alone in HEK cells, and these were efficiently incorporated into cyto-proSAAS spheres when this protein was coexpressed. (D) GFP-TDP-43$^{257\text{-}414}$ exhibits a diffuse cytoplasmic signal when expressed alone but is sequestered by cyto-proSAAS spheres following coexpression. (E) Diagram showing the experimental flow of two TDP-43-inducible HEK cell lines, both transfected with cyto-proSAAS and then induced to express either GFP-TDP-43^{wt} (top) or GFP-TDP-43$^{\Delta NLS}$ (bottom). Cyto-proSAAS sequesters cytoplasmic GFP-TDP-43$^{\Delta NLS}$ but not nuclear GFP-TDP-43^{wt}. PrLD, prion-like domain; RRM, RNA binding domain; NES, nuclear export signal; NLS, nuclear localization signal. Scale bar, 10 μm. Magnified inserts correspond to 10 μm.

43 and maltose binding protein (MBP), a protein tag that greatly favors TDP-43 solubility (Figure 5A). Upon TEV cleavage, TDP-43 undergoes spontaneous aggregation which can be kinetically measured as increased absorbance over time.[38] We found that the TDP-43 fusion protein mixed with a molar excess of proSAAS showed enhanced turbidity as compared to the TDP-43 fusion protein mixed with the same concentration of BSA (Figure 5B). While proSAAS did not become turbid when incubated alone, it is also possible that TDP-43 enhanced its aggregation, thus yielding the increased turbidity results shown here; thus, this assay allows us only to conclude that proSAAS and TDP-43 coaggregate.

Cyto-proSAAS Expression Is Protective against TDP-43 Cytotoxicity. Last, we examined the cytoprotective effects of proSAAS and another neural and endocrine chaperone, 7B2,[39] in a yeast model of TDP-43 toxicity (Figure 6). Genetic modifiers identified in yeast have translated well to higher organisms, for example, in the identification of ataxin-2 knockdown as a potential therapeutic approach for ALS,[40] now in clinical trials. In this model, expression of the full-length TDP-43 and proSAAS transgenes is tightly controlled by a galactose-inducible promoter (pGAL1). The empty vector control showed strong TDP-43-mediated growth impairment on galactose agar after 48 h, whereas this toxicity was partially

https://doi.org/10.1021/acschemneuro.2c00156
ACS Chem. Neurosci. XXXX, XXX, XXX−XXX

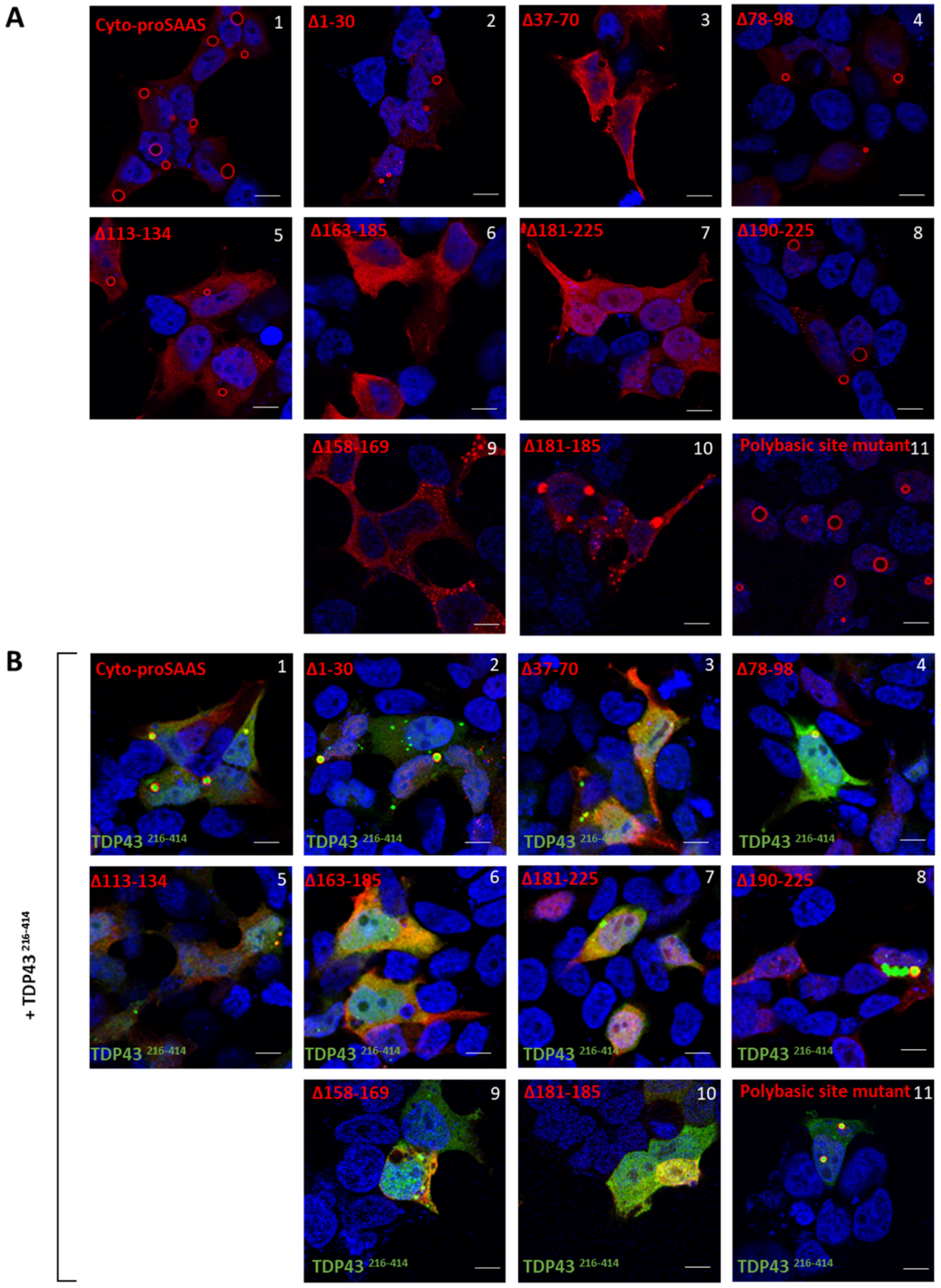

Figure 4. ProSAAS residues 37−70, 158−169, and 181−185 are required for sphere formation with GFP-TDP-43$^{216-414}$ sequestration. (A) Representative images of various deletion constructs of proSAAS expressed in HEK cells showing differences in proSAAS-immunoreactive morphology, ranging from diffuse to punctate to spherical. Scale bar, 20 μm. (B) Representative images of proSAAS deletion constructs coexpressed with GFP-TDP-43$^{216-414}$, showing differences in their ability to sequester GFP-TDP-43$^{216-414}$. Scale bar, 10 μm.

mitigated by expression of proSAAS, cyto-proSAAS, and 7B2. These data provide functional evidence for cytoprotection against full-length TDP-43 toxicity by proSAAS.

DISCUSSION

Prior work has shown that proSAAS, a small unglycosylated secreted chaperone similar in some aspects to heat shock chaperones[39] but which lacks an α-crystallin domain, is able to block and/or prevent the aggregation of peptides and proteins directly involved in neurodegenerative disorders, including amyloid beta 1−42 and α-synuclein.[15−18] ProSAAS, which is predominantly expressed by neurons and endocrine cells, is known to be associated with both extracellular aggregates such as plaques[15] and intracellular aggregates such as Lewy bodies[16]

https://doi.org/10.1021/acschemneuro.2c00156
ACS Chem. Neurosci. XXXX, XXX, XXX−XXX

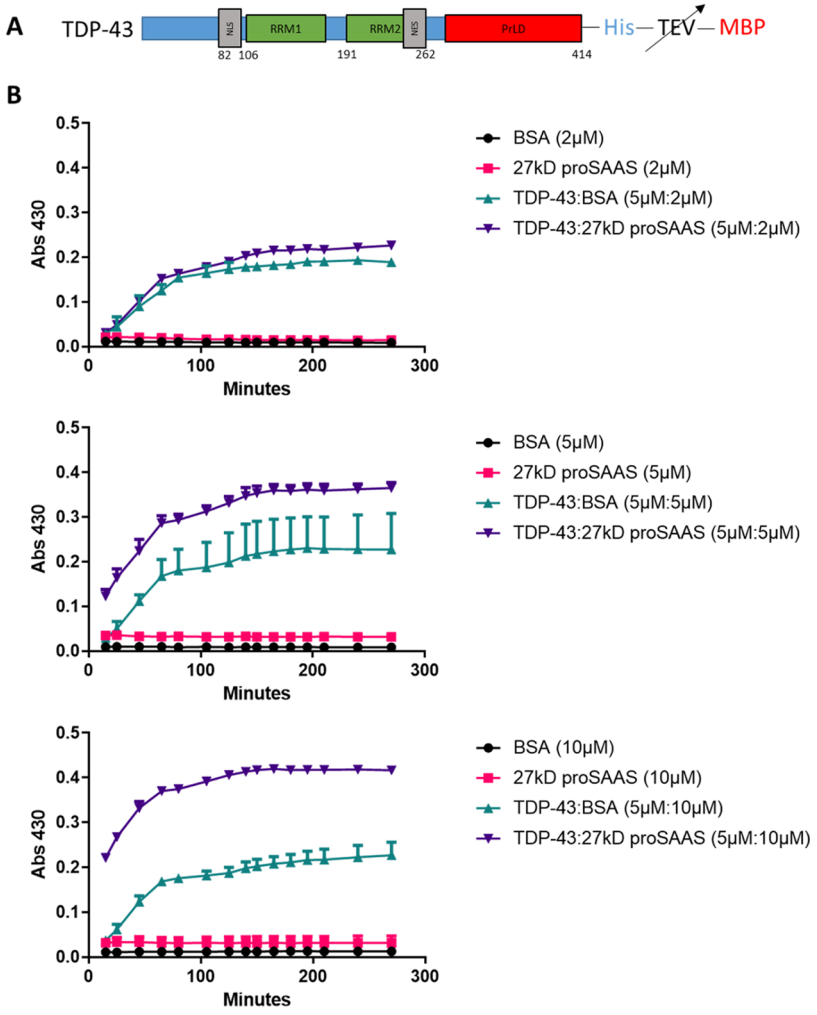

Figure 5. ProSAAS addition to TDP-43 results in enhanced in vitro aggregation. (A) Full-length TDP-43 construct C-terminally tagged with MBP; cleavage of the fusion protein by TEV (arrow) results in TDP-43 aggregation. (B) Graphs depicting the absorbance of proSAAS/BSA alone or mixtures of TDP-43 and proSAAS/BSA at 5 μM:2 μM (top), 5 μM:5 μM (middle), and 5 μM:10 μM (bottom) ratios at 450 nm. ProSAAS addition at a 5 μM:10 μM ratio of TDP-43 to proSAAS greatly increases turbidity relative to the same molar quantity of BSA.

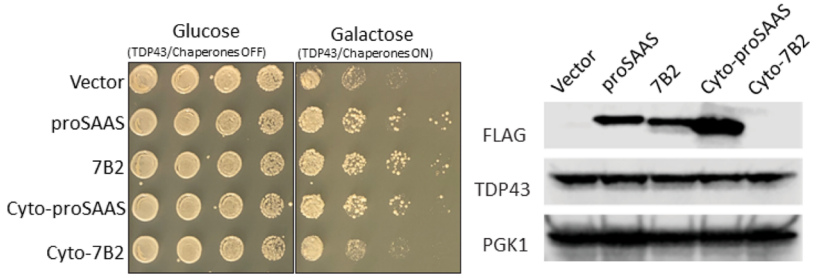

Figure 6. Cyto-proSAAS expression rescues TDP-43 cytotoxicity in a yeast model. A serial dilution spotting assay of yeast expressing full-length TDP-43 and the indicated chaperone from a galactose-inducible promoter is shown. The empty vector is used as a negative control for chaperone activity and shows TDP-43-induced growth impairment on galactose. Left panel: the left side of the spotting plate shows equal spotting and no growth impairment of yeast on glucose media, which does not induce TDP-43 or chaperone expression, while the right side shows growth phenotypes upon induction with galactose. Spotting data are representative images of four independent trials. Right panel: the expression of TDP-43 and chaperones was detected via western blotting; PGK1 (phosphoglycerate kinase 1) was used as a loading control.

and tau aggregates[17,18] in Alzheimer's disease, Parkinson's disease, and FTLD, presumably by uptake from the surrounding medium. ProSAAS has no alternatively spliced forms lacking a signal peptide and thus is unlikely to be directly expressed within the cytoplasm.

In this study, we present data showing that proSAAS self-assembles into spheres both within the secretory pathway and within the cytoplasm. While we do not yet know the role of proSAAS self-assembly within the secretory pathway, we unexpectedly discovered that cytoplasmically expressed pro-SAAS spheres are capable of attracting and sequestering TDP-43

https://doi.org/10.1021/acschemneuro.2c00156
ACS Chem. Neurosci. XXXX, XXX, XXX−XXX

aggregates, including the naturally occurring pathological proteins TDP-43$^{86-414}$ and TDP$^{172-414}$ (TDP-35 and 25, respectively[41]). These synthetic cyto-proSAAS spheres are compact, dense, antibody-impermeable, and formed by progressive fusion of smaller spheres, as clearly shown by dynamic imaging. We initially believed that cyto-proSAAS spheres might constitute a form of stress granule; however, arsenite exposure did not increase their formation, nor were we able to identify any surface association of stress granule markers using traditional reporters for the stress-granule associated RNA-binding proteins G3BP1 or PABPC4. While we were able to demonstrate the homogeneous presence of cyto-proSAAS within the sphere core, whether cyto-proSAAS spheres contain other proteins is technically difficult to establish due to the inability of antibodies to penetrate the sphere shell. Our finding that cyto-proSAAS spheres do not colocalize with Golgi, lysosomal, membrane, and lipid markers supports the idea that the cyto-proSAAS protein itself spontaneously condenses into symmetric spheres with interesting fluid properties.

It is now well established that disordered regions, including disordered prion-like domains, play critical roles in phase transitions that lead to the formation of biomolecular condensates (reviewed in refs 7 and 42). The unusual phase-separating properties of proSAAS also appear to be supported by specific IDDs. While proSAAS does not contain a prion-like domain as predicted by the PLAAC algorithm,[43] it does contain several predicted IDDs and low-complexity domains (Figure S6). We found that amino- and carboxy-terminal IDDs are dispensible for sphere formation but that two other short segments, residues 158−169 and the highly positively charged sequence 181−185, are both required for sphere formation. The first segment represents a well-conserved peptide within proSAAS[16,44] (see also the hidden Markov model shown in the proSAAS Pfam family database PF07259). Interestingly, substitution of lysine for arginines in this latter sequence directs proSAAS expression to the nucleus by apparent formation of a nuclear localization sequence, where it retains its ability to form spheres. These data show that proSAAS has an innate capacity for self-assembly into spheres in three different cellular compartments, suggesting that this property resides solely in its amino acid sequence rather than in compartment-specific factors.

What is the utility of proSAAS spheres artificially expressed within the cytoplasm? Based on the ability of proSAAS to block the aggregation of neurodegeneration-related proteins,[16] we surmised that proSAAS might directly interact with aggregating proteins within the cytoplasm. Indeed, we observed surprisingly efficient entrapment of cytoplasmic GFP-TDP-43$^{216-414}$ aggregates within the cores of cyto-proSAAS spheres. To our knowledge, no similar encapsulated TDP-43-containing particles have been previously reported (reviewed in refs 45 and 46). Screening of other fluorescently tagged potential client proteins indicated that only TDP-43 is able to interact with cyto-proSAAS since cyto-proSAAS spheres did not encapsulate fluorescent forms of HTT, tau, α-Syn, or other non-aggregating cytosolic proteins, including mCherry. Thus, we propose that proSAAS spheres may be useful as a synthetic molecular trap for TDP-43 aggregates.

The TDP-43 protein itself, as well as variants containing disease-causing mutations, is known to form aggregates in FTLD as well as in ALS (reviewed in ref 47), and the prion-like sequence within the carboxy-terminal domain, present in both the full-length and truncated forms TDP-35 and TDP-25, has been identified as a major determinant for TDP-43 aggregation.[41,42,46,48,49] The structure−function studies presented here show that this same prion-like domain is both necessary and sufficient for interactions of TDP-43 with proSAAS spheres. Dynamic imaging of cyto-proSAAS spheres containing fluorescent TDP-43$^{216-414}$ aggregates revealed that cyto-proSAAS spheres containing the GFP-TDP-43$^{216-414}$ cargo undergo progressive fusion and enlargement, supporting the idea that proSAAS spheres can phase-separate even during continuous recruitment of TDP-43 aggregates. In addition, fluorescence derived from internalized GFP-TDP-43 aggregates is signficantly more dispersed (as measured by fluorescence intensity divided by area) than fluorescence derived from external GFP-TDP-43 particles, suggesting direct interactions of internal cyto-proSAAS residues with internalized GFP-TDP-43$^{216-414}$. Aromatic residues play a key role in TDP-43 LLPS;[48,50] these may also be involved in proSAAS interactions. Further studies to identify specific residues within TDP-43$^{216-414}$ that underlie its affinity for chaperones, including synthetic proSAAS spheres, will represent an important step toward management of the aggregative properties of this clinically important protein.

Other synthetic condensates involving TDP-43 aggregates have previously been reported.[51,52] Yu et al. have found that an acetylated, non-RNA-containing form of TDP-43 is able to form dense spherical nuclear annuli ("iLSA") that entrap Hsp70-type chaperones.[52] These TDP43/Hsp70 spheres differ from cyto-proSAAS spheres in three important respects: they require the presence of an energy-dependent chaperone to drive sphere formation; they require the N-terminal domain of TDP-43; and they contain structured assemblies of TDP-43 species as an outer shell for internalized Hsp70, while TDP-43$^{216-414}$ aggregates are sequestered within the cores of cyto-proSAAS spheres. Thus, these Hsp70-containing aggregates represent an inverted assembly as compared to proSAAS spheres, with TDP-43 exposed to the cytoplasm rather than becoming sequestered.

Recent studies have employed synthetic condensates to understand the role of phase separation in cellular processes.[53] Remarkably, the phase-separating bacterial protein PopZ, which has been used to construct short (76-residue) engineered "PopTags" for targeting specific cellular proteins to condensates,[54,55] contains the sequence DVVRELLRPLLKEWL, which is 60% identical to the DVDPELLRYLLGRIL sequence within a conserved proSAAS sequence (residues 153−167). This finding leads us to speculate that a proSAAS-related sequence might conceivably also be employed to construct a mammalian PopTag; in this scenario, cyto-proSAAS could be engineered as a designer "holdase" condensate to reduce the concentration of cytoplasmic aggregates (see also ref 56). The finding that specific lysine substitution directs cyto-proSAAS to the nucleus, where it can also encapsulate truncated TDP-43 forms, may be advantageous in future synthetic biology experiments designed to sequester toxic nuclear aggregates.

Cyto-proSAAS sphere expression clearly results in a variety of functional consequences. First, cyto-proSAAS expression increases the half-life of TDP-43$^{216-414}$, most likely reflecting the sequestration of TDP-43$^{216-414}$ aggregates. We were unable to assess potential protective effects of cyto-proSAAS on TDP-43-mediated cytotoxicity in mammalian cells simply because TDP-43 expression was not consistently cytotoxic in any system we tested, including inducible PC12 cells.[57] However, in yeast cells, cyto-proSAAS partially rescued the growth impairment caused by expression of full-length TDP-43. Previous work on potentiated Hsp104 disaggregases shows that Hsp104-mediated

https://doi.org/10.1021/acschemneuro.2c00156
ACS Chem. Neurosci. XXXX, XXX, XXX−XXX

rescue of aggregate toxicity in yeast models can be replicated in an animal nervous system.[58] Several other modifiers of TDP-43 toxicity in yeast have also translated well to mouse models.[40,59,60] Thus, our findings in yeast are highly promising in their suggestion of cytoprotective effects for proSAAS in higher eukaryotes.

In summary, we have here identified a novel mechanism for aggregate protein sequestration via proSAAS sphere encapsulation. We suggest that further studies exploring the active elements within cyto-proSAAS which interact with TDP-43 will be useful in designing pharmacologic agents and synthetic condensates which are able to enhance aggregate sequestration to therapeutic benefit.

EXPERIMENTAL PROCEDURES

Cell Culture. Neuro2A and HEK cells were obtained from ATCC (Manassas, VA) and grown in OptiMEM/DMEM and DMEM, respectively, both with 10% fetal bovine serum (FBS; Gemini Bio, West Sacramento, CA). Transfection of cells was carried out on 70−80% confluent cells in a 24-well plate fitted with poly-L-lysine-treated glass coverslips using 0.5−1 μg of cDNA and FuGene as per the manufacturer's instructions (Promega, Madison, WI). Cells were fixed for immunocytochemistry 24 or 48 h after transfection, as stated.

Hippocampal primary neurons obtained from E17 rat embryos were cultured as described previously[61] using digestion with 0.25% trypsin−ethylenediaminetetraacetic acid (EDTA) and mechanical dissociation by gentle pipetting through a series of small-bore Pasteur pipettes. Filtered cells were resuspended in a neurobasal medium (Invitrogen) supplemented with 2% B27 supplement, 1% penicillin−streptomycin, and 2 mM GlutaMAX (all from Invitrogen) and then cultured on poly-L-lysine-coated 12 mm coverslips at 37 °C and 5% CO_2 in a humidified atmosphere. Media were replaced every 3−4 days. Seven-day-old primary hippocampal cells, grown on poly-L-lysine-coated 12 mm coverslips, were transfected with 2 μg of cyto-proSAAS cDNA using lipofectamine (Invitrogen). Cells were fixed, immunostained with FLAG and HA tag antisera, and imaged 24 h post transfection. Between 5 and 10% of cells were transfected by this method.

Inducible HEK cells expressing either full-length wild-type or NLS-lacking TDP-43[35] were obtained from Dr. Virginia Lee (University of Pennsylvania). Cells were maintained in DMEM with added GlutaMAX and 10% tetracycline-screened FBS (S10350, Atlanta Biological). Cells were transfected with cyto-proSAAS cDNA as described above and then induced 24 h later with 1 μg/μL of doxycycline (Sigma) for an additional 24 h before fixation and immunostaining.

Expression Vectors. The majority of the constructs used for expressing aggregating proteins were obtained from Addgene (Watertown, MA). The Addgene catalog numbers are as follows: the GFP-tagged TDP-43 constructs TDP-$43^{216-414}$ (#28197), TDP-43^{1-193} (#28202), TDP-43^{1-273} (#28200), TDP-43^{86-414} (#28195), TDP-$43^{170-414}$ (#28196), and TDP-$43^{257-414}$ (#28198), described in ref 31; HTT-Q74 (HTT exon 1 Q74, His- and HA-tagged, #40264) and GFP-HTT-Q74 (#40262) in ref 32; EGFP-Tau (#46904) and EGFP-TauE14 (#46907);[33] and EGFP-α-Syn (#40822) and EGFP-α-Syn-A53T (#40823).[34] The stress granule marker GFP-G3BP1 was also obtained from Addgene (#135997),[62] while the LC3-mCherry construct was obtained from Dr. Marta Lipinksi (U. Maryland-Baltimore; ref 63).

Murine proSAAS, which is 81% identical to human proSAAS, was used in these studies for consistency with previous work.[16] A FLAG-tagged eukaryotic expression vector for murine proSAAS was constructed by Genscript (Piscataway, NJ) in pcDNA3.1(−) (hygromycin-resistant; Invitrogen) by insertion of the nucleotide sequence GATTACAAGGATGACGACGATAAG, encoding the DYKDDDDK FLAG peptide, following the signal peptide. Signal-less cyto-proSAAS was created with a forward primer introducing a methionine amino terminal to the FLAG tag and a reverse primer targeted to the carboxy-terminus of proSAAS. This product was cloned into the *NheI* and *HindIII* sites of the pcDNA3.1(−) hygromycin resistance-encoding vector (Invitrogen). Last, the mCherry proSAAS fusion construct was made by N-terminal insertion of mCherry into the signal-less proSAAS construct. A cytoplasmic mCherry expression vector was obtained from Dr. Megan Rizzo (University of Maryland-Baltimore, MD). All construct sequences were confirmed by sequencing.

Confocal Microscopy. For immunocytochemistry, cells were transfected in a 24-well plate on 12 mm coverslips and fixed in 4% paraformaldehyde (PFA) in PBS for 20 min at 24 or 48 h after transfection, as indicated. Cells were incubated for 30 min at room temperature in IHC blocking buffer (PBS containing 5% FBS, 0.5% Triton X-100 and 100 mM glycine). Antibodies against FLAG (Sigma-Aldrich, #F7425), HSP70 (#11660-T52; Sino Biological), TDP-$43^{216-414}$ (#NB11O-5537; Novus), and GFP (#GFP879484; Aves Labs, Inc) were used at a dilution of 1:1000 in IHC blocking buffer and incubated for 30 min at room temperature. Anti-HA tag antiserum (Abcam, #130275) was incubated with cells overnight at a dilution of 1:200. After washing multiple times with PBS, cells were incubated with secondary fluorescent antibodies (Invitrogen) at a dilution of 1:1000 and Hoechst stain at a dilution of 1:5000. In some experiments, primary antibodies conjugated with fluorescent dyes were used; these were anti-FLAG (Alexa647; #637315; BioLegend), anti-giantin (Alexa488; #908701; BioLegend), and anti-LAMP-1 (Alexa488; #121607; BioLegend). The specificity of the proSAAS signal obtained with anti-FLAG antiserum was confirmed using the IgG-purified antibody raised against the His-tagged, recombinant murine 21 kDa proSAAS protein (proSAAS$^{1-180}$).[15] Morphological characterization of proSAAS spheres and quantitation of the fluorescent signal and transfection efficiency were carried out using Fiji/ImageJ.[64] At least two 40× fields, obtained from three independent experiments using the same experimental conditions, were combined for statistical purposes.

To study the nature of TDP-$43^{216-414}$ aggregates, Z-stacks (0.2 μm intervals) of individual cells expressing TDP-$43^{216-414}$ aggregates, both within and outside cyto-proSAAS spheres, were obtained. For quantitative imaging, 12-bit images were taken, with care to avoid saturation of the GFP signal. The GFP signal within and outside the proSAAS spheres was quantified using 3D ImageJ Suite.[65] Images were first smoothed with a 1.5 pixel Gaussian blur and then segmented in the cyto-proSAAS channel with manual threshold adjustment to select only spheres. The TDP-$43^{216-414}$ channel was segmented with a threshold to include only aggregated GFP signals. Binary masks were generated using the segmented images and used to quantify the original GFP signal inside and outside the cyto-proSAAS sphere using the Measure 3D and Quant 3D plugins.

STED Microscopy. HEK cells were plated on 12 mm coverslips at 70−80% confluency and transfected with sec-proSAAS or cyto-proSAAS cDNAs. After 24 h, the coverslips were fixed and immunostained using the homemade anti-proSAAS antibody as described before and the STAR-RED secondary antibody compatible with STED microscopy. A Nikon A1RHD25/STED microscope was used to generate super-resolution images of proSAAS spheres.

Dynamic In Vivo Imaging. Live cell confocal microscopy was performed on a Nikon W1 spinning disk confocal system on a Nikon Ti2 inverted microscope, with a Hamamatsu sCMOS camera, at the Confocal Microscopy Core Facility, University of Maryland Baltimore. Acquisition was controlled with Nikon Elements software. Cells were incubated at 37 °C and under 5% CO_2 in Opti-MEM media during imaging. Cells were grown in high grid 500 35 mm plates (Ibidi; Fitchburg, WI) to 50% confluence and double- (TDP-$43^{216-414}$ and cyto-proSAAS; equal ratio) or triple-transfected (TDP-$43^{216-414}$, cyto-proSAAS, and mCherry cyto-proSAAS; 1, 1, and 0.2 μg, respectively) for 6−24 h prior to imaging GFP and mCherry fluorescence, as indicated in the figures. Live cell DIC and epi-fluorescent microscopy was performed on an Olympus VivaView. Cells were plated in 35 mm glass-bottomed dishes (MatTek; Ashland, MA) and transfected 18 h prior to the start of imaging. Multiple regions of cells were selected and imaged at 2 min intervals over a period of 6 h using excitation/emission filter sets for GFP and RFP. Image analysis was performed with ImageJ. For cyto-proSAAS dynamic imaging HEK cells were grown to 50%

https://doi.org/10.1021/acschemneuro.2c00156
ACS Chem. Neurosci. XXXX, XXX, XXX−XXX

confluency on a 35 × 10 mm^2 glass bottom (170 μm) TC-treated Eppendorf cell imaging dish (E0030740017), incubated for 18 h after transfection with 0.2 μg of mCherry-cyto-proSAAS and 1 μg of cyto-proSAAS, and then imaged using a Nikon A1RHD25 microscope for 17 h using the same incubation conditions as described above. The movie was converted to a fast format using Nikon A1 confocal software.

Electron Microscopy. HEK 293 cells were grown on 12 mm coverslips up to 70% confluency and transfected with the empty vector, TDP-43$^{216-414}$ cDNA alone, or TDP-43$^{216-414}$ in combination with cyto-proSAAS cDNA. 24 h after transfection, cells were fixed in a solution of 2% paraformaldehyde and 2.5% glutaraldehyde in 0.1 M piperazine-*N*,*N*′-bis(2-ethanesulfonic acid) (PIPES) buffer (pH 7). After washing, cells were quenched with 50 mM glycine in 0.1 M PIPES buffer (pH 7) for 15 min and washed again with 0.1 M PIPES buffer, post-fixed in 1% (w/v) osmium tetroxide and 0.75% ferrocyanide in 0.1 M PIPES buffer for 60 min, washed with 0.1 M PIPES, and stained with 1% (w/v) uranyl acetate in water for 30 min. After washing, specimens were dehydrated using serially graded ethanol solutions (30, 50, 70, 90, and 100%) and infiltrated and embedded in Spurs resin (Electron Microscopy Sciences, Hatfield, PA) following the manufacturer's recommendations. Ultrathin sections (70 nm) were cut on a Leica UC6 ultramicrotome (Leica Microsystems, Inc., Bannockburn, IL), collected onto copper grids, and examined on a Tecnai T12 transmission electron microscope [Thermo Fisher (Formerly FEI. Co.), Hillsboro, OR] operated at 80 kEV. Digital images were acquired by using a bottom-mounted CCD camera (Advanced Microscopy Techniques, Corp, Woburn, MA) and AMT600 software.

Western Blotting. Western blotting of HEK cell extracts was performed using 70−80% confluent cells grown in 12-well plates. Cells were resuspended in 150 μL of RIPA buffer [25 mM Tris pH 7−8, 150 mM NaCl, 0.1% sodium dodecyl sulfate (SDS), 1% Triton X-100, and 0.5% sodium deoxycholate, supplemented with protease inhibitors ("complete"; Sigma-Aldrich, St. Louis, MO)] and frozen prior to assay. Samples were thawed, boiled, electrophoresed on 15% acrylamide gels, and blotted to nitrocellulose using a BioRad Turbo Blotter at 25 V for 10 min. Blots were blocked in 5% blotting grade milk (Bio-Rad) in 0.05% Tween-20 in Tris-buffered saline, pH 7.4 (blotting buffer), and were then incubated with primary antisera against GFP (1:1500; #879484; Aves Labs, Inc), anti-FLAG (Sigma-Aldrich, #F7425), or anti-actin (#A2228; Sigma) in the blotting buffer overnight at 4 C. Secondary antisera, used at dilutions of 1:5000 in the blocking buffer, were horseradish peroxidase-linked (Bio-Rad #s170-6516, 170-6615, and L005680A, respectively).

Cycloheximide Experiments. HEK cells were plated in 12-well plates and transfected when 70−80% confluence was reached. Cycloheximide (20 μg/mL; Sigma-Aldrich) was used to inhibit total protein synthesis 24 h after transfection. The cells were monitored for 6 h following addition of the drug, a duration that resulted in 80% reduction of aggregates in cells transfected with GFP-TDP-43$^{216-414}$. Cells were lysed in Laemmli sample buffer at the times indicated in the Results section and subjected to blotting using chicken antiserum against GFP (Aves Labs). Three independent experiments were used for quantification purposes. To investigate the cellular distribution of proteins following 6 h of cycloheximide treatment, cells were fixed as previously described, immunostained using the anti-FLAG antibody (Sigma-Aldrich, #F7425), and imaged by confocal microscopy.

Bioinformatics and Site-Directed Mutagenesis for Structure−Function Studies. The cyto-proSAAS amino acid sequence was analyzed using the online tools Predictor of Natural Disordered Regions (PONDR) for intrinsically disordered domains (IDDs) and PLAtform of TOols for LOw Complexity (PlaToLoCo) using the SEG tool for low-complexity regions. Helices and coils were predicted using online software AlphaFold[66,67] and DeepCoil.[68] Based on this analysis, a series of FLAG-tagged cyto-proSAAS constructs lacking the sequences encoding the amino acids 1−30, 37−70, 78−98, 113−134, 163−185, 181−225, or 190−225 were generated using site-directed mutagenesis and cloned into pcDNA3.1(−) by Genscript (Piscataway, NJ) for eukaryotic expression. In addition, three other constructs, the first lacking a specific conserved region (residues 158−169),[16] the second lacking the polybasic site (residues 181−185), and the third containing five mutations replacing RRLRR with KKAKK in this same polybasic site (replacing CGCCGCCTCCGCCGA with AAAAAGG-CAAAAAAG), were generated by Genscript (Piscataway, NJ). All constructs were verified by bidirectional cDNA sequencing. Vectors were transfected either alone or together with a vector encoding GFP-TDP-43$^{216-414}$ into 70−80% confluent HEK cells. Cells were fixed and immunostained with anti-FLAG antiserum (Alexa647; #637315; BioLegend) and Hoechst dye to assess cyto-proSAAS sphere formation and TDP-43 sequestration 24 h after transfection. Mean intensities and sphere dimensions were measured using ImageJ software. Cell counts were performed manually.

Protein Purification and In Vitro TDP-43 Aggregation Assay. The pJ4M/TDP-43 vector encoding 6xHis-TDP-43-TEV-MBP was obtained from Addgene (#104480; ref 37). A His-tagged proSAAS cDNA (lacking the signal peptide) was cloned into pET45a(−) using a GoTaq Flexi DNA Polymerase kit (M829). Starter cultures of *Escherichia coli* BL21 DE3 cells, transformed with each construct, were used to inoculate 1 L of the autoinduction medium containing NPS [0.025 M $(NH_4)_2SO_4$, 0.05 M KH_2PO_4, and 0.05 M Na_2HPO_4] and 50/5/2 (0.5% glycerol, 0.05% glucose, and 0.02% lactose) and incubated overnight at 30 °C at 210 rpm for expression by autoinduction. The TDP-43 fusion protein was purified from cell extracts using Ni−nitrilotriacetic acid (Ni-NTA) and amylose affinity chromatography following published protocols.[37,38] Recombinant proSAAS was purified by Ni-NTA affinity chromatography, as previously described.[16]

To perform the in vitro TDP-43 aggregation assay, the TDP-43-TEV-MBP fusion protein was first exchanged into the aggregation buffer [20 mM *N*-(2-hydroxyethyl)piperazine-*N*′-ethanesulfonic acid (Hepes), pH 7.0, 150 mM NaCl, and 1 mM DTT] and centrifuged, as previously described.[38] The final concentrations of 5 μM TDP-43-TEV-MBP and the indicated final concentrations of recombinant proSAAS or BSA (NEB BioLabs; B9001S) were achieved by mixing aliquots of a 44 μM stock solution of TDP-43-TEV-MBP with aliquots of stock solutions of either 55 μM proSAAS or 151 μM BSA (both in 5 mM acetic acid). These solutions were added to 100 units of TEV protease (NEB) in the aggregation buffer, present in black-walled 96-well clear-bottom plates (Costar #3904). The assay was carried out in triplicate in a total volume of 100 μL of the aggregation buffer; control wells contained only proSAAS or BSA and TEV in the same volume of the aggregation buffer. The absorbance was measured at 450 nm using a BioRad plate spectrophotometer every 15 min over 5 h.

Yeast Cell Screen for ProSAAS/cyto-proSAAS Rescue from TDP-43 Cytotoxicity. Yeast experiments were performed using the BY4741Δhsp104 strain. Expression of TDP-43 was induced from the pGAL1 promoter, which is maintained on a HIS3-selectable CEN plasmid (pEB413GAL_TDP-43). ProSAAS and 7B2 (and their signal-less forms) were expressed from pGAL1 on a separate URA3-selectable CEN plasmid (pEB416GAL). Prior to the yeast spotting assays and western blotting, the yeast were cultured for 12 h at 30 °C in pre-induction media containing 2% raffinose + synthetic-defined media lacking histidine and uracil (-his/ura). For spotting assays, the samples were normalized to an OD_{600} of 2 and serially diluted fivefold per spot. Rescue of TDP-43 cytotoxicity was assessed after 48 h of spot growth on 2% glucose or galactose his/ura agar plates at 30 °C. For western blotting, the yeast were inoculated in liquid induction media containing 2% galactose his/ura and grown for 6 h to induce protein expression. Normalized cell pellets were treated for 5 min with 0.1 M NaOH, followed by resuspension in 1× SDS-PAGE sample buffer (100 mM Tris-HCl pH 6.8, 4 mM EDTA, 4% SDS, 0.1% bromophenol blue, 20% glycerol) + fungal protease inhibitor cocktail (Sigma, P8215), and then heated at 95 °C for 10 min. Samples were electrophoresed on a 4−20% Criterion Precast Tris-HCl acrylamide gel (200 V for 1 h) and transferred to a PVDF membrane (0.15 A for 1 h). Blots were blocked with Li-COR Odyssey Blocking Buffer and then incubated with primary antibodies: anti-FLAG (Sigma F1804, 1:1000 for proSAAS and 7B2), anti-TDP-43 (Proteintech 10782-2-AP, 1:1000), or anti-PGK1 (Invitrogen 459250, 1:1000). Blots were visualized after 30 min incubation with secondary antibodies (Li-COR 680RD anti-rabbit 1:2500, Li-COR 800CW anti-mouse 1:5000).

https://doi.org/10.1021/acschemneuro.2c00156
ACS Chem. Neurosci. XXXX, XXX, XXX−XXX

Statistical Analysis. We used GraphPad Prism 5.0 and 6.0 (GraphPad Software, La Jolla, USA) for statistical analyses and data presentation. Graphs represent means ± standard deviation (SD) or standard error (SE), as indicated, with the number of replicates indicated in the Methods section or Figure Legends. Student's unpaired two-tailed *t*-test was used for comparison of data obtained for fluorescence density measurements from at least three independent experiments, with $p < 0.05$ considered significant.

■ ASSOCIATED CONTENT

Supporting Information

The Supporting Information is available free of charge at https://pubs.acs.org/doi/10.1021/acschemneuro.2c00156.

Cyto-proSAAS expressed in different cell types including hippocampal neurons; cyto-proSAAS expressed together with tagged forms of other aggregating proteins including Huntingtin, synuclein, and mutants of both proteins; dynamic fusion of cyto-proSAAS spheres in the presence and absence of coexpressed GFP-TDP-43$^{212-414}$; data on the lack of colocalization of proSAAS spheres with markers of membranes, lipids, stress granules, and other cellular organelles; cellular TDP-43 levels assessed by blotting as well as the fluorescence density of GFP-TDP-43 measured after cycloheximide treatment in the presence and absence of proSAAS; structure−function studies showing the lack of proSAAS encapsulation of the N-terminal portions of GFP-TDP-43; disorder predictions for the proSAAS sequence; and quality control information for the purified proteins used in the article including TDP-43-MBP and His-tagged proSAAS (PDF)

Dynamic imaging of mCherry-cyto-proSAAS spheres showing fusion of large spheres (AVI)

Dynamic imaging of mCherry-cyto-proSAAS spheres showing sphere fusion with simultaneous GFP-TDP-43$^{216-414}$ (AVI)

■ AUTHOR INFORMATION

Corresponding Author

Iris Lindberg − *Department of Anatomy and Neurobiology, University of Maryland School of Medicine, University of Maryland, Baltimore, Maryland 21201, United States;* orcid.org/0000-0002-1188-170X; Email: ilindberg@som.umaryland.edu

Authors

Juan R. Peinado − *Department of Anatomy and Neurobiology, University of Maryland School of Medicine, University of Maryland, Baltimore, Maryland 21201, United States;* Present Address: Department of Medical Sciences, Ciudad Real Medical School, Oxidative Stress and Neurodegeneration Group, Regional Center for Biomedical Research, University of Castilla-La Mancha (UCLM), Ciudad Real, Spain

Kriti Chaplot − *Department of Anatomy and Neurobiology, University of Maryland School of Medicine, University of Maryland, Baltimore, Maryland 21201, United States*

Timothy S. Jarvela − *Department of Anatomy and Neurobiology, University of Maryland School of Medicine, University of Maryland, Baltimore, Maryland 21201, United States*

Edward M. Barbieri − *Department of Biochemistry and Biophysics, Perelman School of Medicine, University of Pennsylvania, Philadelphia, Pennsylvania 19104, United States*

James Shorter − *Department of Biochemistry and Biophysics, Perelman School of Medicine, University of Pennsylvania, Philadelphia, Pennsylvania 19104, United States;* orcid.org/0000-0001-5269-8533

Complete contact information is available at: https://pubs.acs.org/10.1021/acschemneuro.2c00156

Author Contributions

#J.P. and K.C. contributed equally. Experiments were carried out by J.P., K.C., T.S.J., and E.B. and supervised by I.L. and J.S. The manuscript was written by K.C., J.P., E.B., and I.L. and was reviewed by all authors.

Notes

The authors declare no competing financial interest.

■ ACKNOWLEDGMENTS

We are grateful for research support from NIH grant AG 0062222 to I.L. and support from "*Convocatorias de movilidad*" from the University of Castilla-la Mancha (UCLM) to J.R.P. This work utilized an EM sample preparation instrument that was purchased with funding from a National Institutes of Health SIG grant (1S10RR26870-1). We are grateful for the assistance of Dr. Ru-ching Hsia of the Electron Microscopy Core Imaging Facility, Center for Innovative Biomedical Resources, University of Maryland-Baltimore. We acknowledge the use of the Confocal Microscopy Core Facility, University of Maryland-Baltimore. We thank Ms. Minerva Contreras for hippocampal neurons and our UMB colleagues Drs. Rizzo and Lipinski for various constructs. We thank Dr. Bede Portz for help with the MBP-TDP-43 aggregation assay. We thank Dr. Virginia Lee for providing the inducible TDP-43 HEK cells and are grateful to Mr. Nicholas Schaffer for helping with image analysis. E.B. was supported by a Milton Safenowitz Post-Doctoral Fellowship from ALSA and by NIH grant F32NS108598. J.S. was supported by grants from ALSA, target ALS, and The Robert Packard Center for ALS Research at Johns Hopkins.

■ REFERENCES

(1) Valastyan, J. S.; Lindquist, S. Mechanisms of protein-folding diseases at a glance. *Dis. Models Mech.* **2014**, *7*, 9−14.

(2) Klaips, C. L.; Jayaraj, G. G.; Hartl, F. U. Pathways of cellular proteostasis in aging and disease. *J. Cell Biol.* **2018**, *217*, 51−63.

(3) Ayala, Y. M.; Zago, P.; D'Ambrogio, A.; Xu, Y. F.; Petrucelli, L.; Buratti, E.; Baralle, F. E. Structural determinants of the cellular localization and shuttling of TDP-43. *J. Cell Sci.* **2008**, *121*, 3778−3785.

(4) Neumann, M.; Sampathu, D. M.; Kwong, L. K.; Truax, A. C.; Micsenyi, M. C.; Chou, T. T.; Bruce, J.; Schuck, T.; Grossman, M.; Clark, C. M.; McCluskey, L. F.; Miller, B. L.; Masliah, E.; Mackenzie, I. R.; Feldman, H.; Feiden, W.; Kretzschmar, H. A.; Trojanowski, J. Q.; Lee, V. M.-Y. Ubiquitinated TDP-43 in frontotemporal lobar degeneration and amyotrophic lateral sclerosis. *Science* **2006**, *314*, 130−133.

(5) de Boer, E. M. J.; Orie, V. K.; Williams, T.; Baker, M. R.; De Oliveira, H. M.; Polvikoski, T.; Silsby, M.; Menon, P.; van den Bos, M.; Halliday, G. M.; van den Berg, L. H.; Van Den Bosch, L.; van Damme, P.; Kiernan, M. C.; van Es, M. A.; Vucic, S. TDP-43 proteinopathies: a new wave of neurodegenerative diseases. *J. Neurol. Neurosurg. Psychiatry* **2020**, *92*, 86−95.

(6) Gasset-Rosa, F.; Lu, S.; Yu, H.; Chen, C.; Melamed, Z. e.; Guo, L.; Shorter, J.; Da Cruz, S.; Cleveland, D. W. Cytoplasmic TDP-43 De-mixing Independent of Stress Granules Drives Inhibition of Nuclear

Import, Loss of Nuclear TDP-43, and Cell Death. *Neuron* **2019**, *102*, 339−357.
(7) Gomes, E.; Shorter, J. The molecular language of membraneless organelles. *J. Biol. Chem.* **2019**, *294*, 7115−7127.
(8) Hartl, F. U. Protein Misfolding Diseases. *Annu. Rev. Biochem.* **2017**, *86*, 21−26.
(9) Bobori, C.; Theocharopoulou, G.; Vlamos, P. Molecular Chaperones in Neurodegenerative Diseases: A Short Review. *Adv. Exp. Med. Biol.* **2017**, *987*, 219−231.
(10) Chiti, F.; Dobson, C. M. Protein Misfolding, Amyloid Formation, and Human Disease: A Summary of Progress Over the Last Decade. *Annu. Rev. Biochem.* **2017**, *86*, 27−68.
(11) Balchin, D.; Hayer-Hartl, M.; Hartl, F. U. In vivo aspects of protein folding and quality control. *Science* **2016**, *353*, aac4354.
(12) Webster, J. M.; Darling, A. L.; Uversky, V. N.; Blair, L. J. Small Heat Shock Proteins, Big Impact on Protein Aggregation in Neurodegenerative Disease. *Front. Pharmacol.* **2019**, *10*, 1047.
(13) Whiten, D. R.; Cox, D.; Horrocks, M. H.; Taylor, C. G.; De, S.; Flagmeier, P.; Tosatto, L.; Kumita, J. R.; Ecroyd, H.; Dobson, C. M.; Klenerman, D.; Wilson, M. R. Single-Molecule Characterization of the Interactions between Extracellular Chaperones and Toxic alpha-Synuclein Oligomers. *Cell Rep.* **2018**, *23*, 3492−3500.
(14) Foster, E. M.; Dangla-Valls, A.; Lovestone, S.; Ribe, E. M.; Buckley, N. J. Clusterin in Alzheimer's Disease: Mechanisms, Genetics, and Lessons From Other Pathologies. *Front. Neurosci.* **2019**, *13*, 164.
(15) Hoshino, A.; Helwig, M.; Rezaei, S.; Berridge, C.; Eriksen, J. L.; Lindberg, I. A novel function for proSAAS as an amyloid anti-aggregant in Alzheimer's disease. *J. Neurochem.* **2014**, *128*, 419−430.
(16) Jarvela, T. S.; Lam, H. A.; Helwig, M.; Lorenzen, N.; Otzen, D. E.; McLean, P. J.; Maidment, N. T.; Lindberg, I. The neural chaperone proSAAS blocks alpha-synuclein fibrillation and neurotoxicity. *Proc. Natl. Acad. Sci. U. S. A.* **2016**, *113*, E4708−E4715.
(17) Kikuchi, K.; Arawaka, S.; Koyama, S.; Kimura, H.; Ren, C.-H.; Wada, M.; Kawanami, T.; Kurita, K.; Daimon, M.; Kawakatsu, S.; Kadoya, T.; Goto, K.; Kato, T. An N-terminal fragment of ProSAAS (a granin-like neuroendocrine peptide precursor) is associated with tau inclusions in Pick's disease. *Biochem. Biophys. Res. Commun.* **2003**, *308*, 646−654.
(18) Wada, M.; Ren, C.-H.; Koyama, S.; Arawaka, S.; Kawakatsu, S.; Kimura, H.; Nagasawa, H.; Kawanami, T.; Kurita, K.; Daimon, M.; Hirano, A.; Kato, T. A human granin-like neuroendocrine peptide precursor (proSAAS) immunoreactivity in tau inclusions of Alzheimer's disease and parkinsonism-dementia complex on Guam. *Neurosci. Lett.* **2004**, *356*, 49−52.
(19) Davidsson, P.; Sjögren, M.; Andreasen, N.; Lindbjer, M.; Nilsson, C. L.; Westman-Brinkmalm, A.; Blennow, K. Studies of the pathophysiological mechanisms in frontotemporal dementia by proteome analysis of CSF proteins. *Mol. Brain Res.* **2002**, *109*, 128−133.
(20) Abdi, F.; Quinn, J. F.; Jankovic, J.; McIntosh, M.; Leverenz, J. B.; Peskind, E.; Nixon, R.; Nutt, J.; Chung, K.; Zabetian, C.; Samii, A.; Lin, M.; Hattan, S.; Pan, C.; Wang, Y.; Jin, J.; Zhu, D.; Li, G. J.; Liu, Y.; Waichunas, D.; Montine, T. J.; Zhang, J. Detection of biomarkers with a multiplex quantitative proteomic platform in cerebrospinal fluid of patients with neurodegenerative disorders. *J. Alzheimer's Dis.* **2006**, *9*, 293−348.
(21) Jahn, H.; Wittke, S.; Zürbig, P.; Raedler, T. J.; Arlt, S.; Kellmann, M.; Mullen, W.; Eichenlaub, M.; Mischak, H.; Wiedemann, K. Peptide fingerprinting of Alzheimer's disease in cerebrospinal fluid: identification and prospective evaluation of new synaptic biomarkers. *PLoS One* **2011**, *6*, No. e26540.
(22) Finehout, E. J.; Franck, Z.; Choe, L. H.; Relkin, N.; Lee, K. H. Cerebrospinal fluid proteomic biomarkers for Alzheimer's disease. *Ann. Neurol.* **2007**, *61*, 120−129.
(23) Wang, J.; Cunningham, R.; Zetterberg, H.; Asthana, S.; Carlsson, C.; Okonkwo, O.; Li, L. Label-free quantitative comparison of cerebrospinal fluid glycoproteins and endogenous peptides in subjects with Alzheimer's disease, mild cognitive impairment, and healthy individuals. *Proteonomics Clin. Appl.* **2016**, *10*, 1225−1241.
(24) Choi, Y. S.; Hou, S.; Choe, L. H.; Lee, K. H. Targeted human cerebrospinal fluid proteomics for the validation of multiple Alzheimer's disease biomarker candidates. *J. Chromatogr. B: Anal. Technol. Biomed. Life Sci.* **2013**, *930*, 129−135.
(25) Spellman, D. S.; Wildsmith, K. R.; Honigberg, L. A.; Tuefferd, M.; Baker, D.; Raghavan, N.; Nairn, A. C.; Croteau, P.; Schirm, M.; Allard, R.; Lamontagne, J.; Chelsky, D.; Hoffmann, S.; Potter, W. Z. Development and evaluation of a multiplexed mass spectrometry based assay for measuring candidate peptide biomarkers in Alzheimer's Disease Neuroimaging Initiative (ADNI) CSF. *Proteonomics Clin. Appl.* **2015**, *9*, 715−731.
(26) Hölttä, M.; Minthon, L.; Hansson, O.; Holmén-Larsson, J.; Pike, I.; Ward, M.; Kuhn, K.; Rüetschi, U.; Zetterberg, H.; Blennow, K.; Gobom, J. An integrated workflow for multiplex CSF proteomics and peptidomics-identification of candidate cerebrospinal fluid biomarkers of Alzheimer's disease. *J. Proteome Res.* **2015**, *14*, 654−663.
(27) Khoonsari, P. E.; Shevchenko, G.; Herman, S.; Remnestål, J.; Giedraitis, V.; Brundin, R.; Degerman Gunnarsson, M.; Kilander, L.; Zetterberg, H.; Nilsson, P.; Lannfelt, L.; Ingelsson, M.; Kultima, K. Improved Differential Diagnosis of Alzheimer's Disease by Integrating ELISA and Mass Spectrometry-Based Cerebrospinal Fluid Biomarkers. *J. Alzheimer's Dis.* **2019**, *67*, 639−651.
(28) van Steenoven, I.; Koel-Simmelink, M. J. A.; Vergouw, L. J. M.; Tijms, B. M.; Piersma, S. R.; Pham, T. V.; Bridel, C.; Ferri, G.-L.; Cocco, C.; Noli, B.; Worley, P. F.; Xiao, M.-F.; Xu, D.; Oeckl, P.; Otto, M.; van der Flier, W. M.; de Jong, F. J.; Jimenez, C. R.; Lemstra, A. W.; Teunissen, C. E. Identification of novel cerebrospinal fluid biomarker candidates for dementia with Lewy bodies: a proteomic approach. *Mol. Neurodegener.* **2020**, *15*, 36.
(29) Mathys, H.; Davila-Velderrain, J.; Peng, Z.; Gao, F.; Mohammadi, S.; Young, J. Z.; Menon, M.; He, L.; Abdurrob, F.; Jiang, X.; Martorell, A. J.; Ransohoff, R. M.; Hafler, B. P.; Bennett, D. A.; Kellis, M.; Tsai, L.-H. Single-cell transcriptomic analysis of Alzheimer's disease. *Nature* **2019**, *570*, 332−337.
(30) Dörrbaum, A. R.; Alvarez-Castelao, B.; Nassim-Assir, B.; Langer, J. D.; Schuman, E. M. Proteome dynamics during homeostatic scaling in cultured neurons. *Elife* **2020**, *9*, No. e52939.
(31) Yang, C.; Tan, W.; Whittle, C.; Qiu, L.; Cao, L.; Akbarian, S.; Xu, Z. The C-terminal TDP-43 fragments have a high aggregation propensity and harm neurons by a dominant-negative mechanism. *PLoS One* **2010**, *5*, No. e15878.
(32) Narain, Y.; Wyttenbach, A.; Rankin, J.; Furlong, R. A.; Rubinsztein, D. C. A molecular investigation of true dominance in Huntington's disease. *J. Med. Genet.* **1999**, *36*, 739−746.
(33) Hoover, B. R.; Reed, M. N.; Su, J.; Penrod, R. D.; Kotilinek, L. A.; Grant, M. K.; Pitstick, R.; Carlson, G. A.; Lanier, L. M.; Yuan, L.-L.; Ashe, K. H.; Liao, D. Tau mislocalization to dendritic spines mediates synaptic dysfunction independently of neurodegeneration. *Neuron* **2010**, *68*, 1067−1081.
(34) Furlong, R. A.; Narain, Y.; Rankin, J.; Wyttenbach, A.; Rubinsztein, D. C. Alpha-synuclein overexpression promotes aggregation of mutant huntingtin. *Biochem. J.* **2000**, *346*, 577−581.
(35) Porta, S.; Xu, Y.; Restrepo, C. R.; Kwong, L. K.; Zhang, B.; Brown, H. J.; Lee, E. B.; Trojanowski, J. Q.; Lee, V. M.-Y. Patient-derived frontotemporal lobar degeneration brain extracts induce formation and spreading of TDP-43 pathology in vivo. *Nat. Commun.* **2018**, *9*, 4220.
(36) Jarnot, P.; Ziemska-Legiecka, J.; Dobson, L.; Merski, M.; Mier, P.; Andrade-Navarro, M. A.; Hancock, J. M.; Dosztányi, Z.; Paladin, L.; Necci, M.; Piovesan, D.; Tosatto, S. C. E.; Promponas, V. J.; Grynberg, M.; Gruca, A. PlaToLoCo: the first web meta-server for visualization and annotation of low complexity regions in proteins. *Nucleic Acids Res.* **2020**, *48*, W77−w84.
(37) Wang, A.; Conicella, A. E.; Schmidt, H. B.; Martin, E. W.; Rhoads, S. N.; Reeb, A. N.; Nourse, A.; Ramirez Montero, D.; Ryan, V. H.; Rohatgi, R.; Shewmaker, F.; Naik, M. T.; Mittag, T.; Ayala, Y. M.; Fawzi, N. L. A single N-terminal phosphomimic disrupts TDP-43 polymerization, phase separation, and RNA splicing. *EMBO J.* **2018**, *37*, No. e97452.

https://doi.org/10.1021/acschemneuro.2c00156
ACS Chem. Neurosci. XXXX, XXX, XXX−XXX

(38) Mann, J. R.; Gleixner, A. M.; Mauna, J. C.; Gomes, E.; DeChellis-Marks, M. R.; Needham, P. G.; Copley, K. E.; Hurtle, B.; Portz, B.; Pyles, N. J.; Guo, L.; Calder, C. B.; Wills, Z. P.; Pandey, U. B.; Kofler, J. K.; Brodsky, J. L.; Thathiah, A.; Shorter, J.; Donnelly, C. J. RNA Binding Antagonizes Neurotoxic Phase Transitions of TDP-43. *Neuron* **2019**, *102*, 321−338.
(39) Chaplot, K.; Jarvela, T. S.; Lindberg, I. Secreted Chaperones in Neurodegeneration. *Front. Aging Neurosci.* **2020**, *12*, 268.
(40) Becker, L. A.; Huang, B.; Bieri, G.; Ma, R.; Knowles, D. A.; Jafar-Nejad, P.; Messing, J.; Kim, H. J.; Soriano, A.; Auburger, G.; Pulst, S. M.; Taylor, J. P.; Rigo, F.; Gitler, A. D. Therapeutic reduction of ataxin-2 extends lifespan and reduces pathology in TDP-43 mice. *Nature* **2017**, *544*, 367−371.
(41) Suk, T. R.; Rousseaux, M. W. C. The role of TDP-43 mislocalization in amyotrophic lateral sclerosis. *Mol. Neurodegener.* **2020**, *15*, 45.
(42) Banani, S. F.; Lee, H. O.; Hyman, A. A.; Rosen, M. K. Biomolecular condensates: organizers of cellular biochemistry. *Nat. Rev. Mol. Cell Biol.* **2017**, *18*, 285−298.
(43) Alberti, S.; Halfmann, R.; King, O.; Kapila, A.; Lindquist, S. A systematic survey identifies prions and illuminates sequence features of prionogenic proteins. *Cell* **2009**, *137*, 146−158.
(44) Kudo, H.; Liu, J.; Jansen, E. J. R.; Ozawa, A.; Panula, P.; Martens, G. J. M.; Lindberg, I. Identification of proSAAS homologs in lower vertebrates: conservation of hydrophobic helices and convertase-inhibiting sequences. *Endocrinology* **2009**, *150*, 1393−1399.
(45) Wolozin, B.; Ivanov, P. Stress granules and neurodegeneration. *Nat. Rev. Neurosci.* **2019**, *20*, 649−666.
(46) Prasad, A.; Bharathi, V.; Sivalingam, V.; Girdhar, A.; Patel, B. K. Molecular Mechanisms of TDP-43 Misfolding and Pathology in Amyotrophic Lateral Sclerosis. *Front. Mol. Neurosci.* **2019**, *12*, 25.
(47) Eck, R. J.; Kraemer, B. C.; Liachko, N. F. Regulation of TDP-43 phosphorylation in aging and disease. *Geroscience* **2021**, *43*, 1605−1614.
(48) Schmidt, H. B.; Barreau, A.; Rohatgi, R. Phase separation-deficient TDP43 remains functional in splicing. *Nat. Commun.* **2019**, *10*, 4890.
(49) Johnson, B. S.; Snead, D.; Lee, J. J.; McCaffery, J. M.; Shorter, J.; Gitler, A. D. TDP-43 is intrinsically aggregation-prone, and amyotrophic lateral sclerosis-linked mutations accelerate aggregation and increase toxicity. *J. Biol. Chem.* **2009**, *284*, 20329−20339.
(50) Li, H.-R.; Chiang, W.-C.; Chou, P.-C.; Wang, W.-J.; Huang, J.-r. TAR DNA-binding protein 43 (TDP-43) liquid-liquid phase separation is mediated by just a few aromatic residues. *J. Biol. Chem.* **2018**, *293*, 6090−6098.
(51) Schmidt, H. B.; Rohatgi, R. Vivo Formation of Vacuolated Multi-phase Compartments Lacking Membranes. *Cell Rep.* **2016**, *16*, 1228−1236.
(52) Yu, H.; Lu, S.; Gasior, K.; Singh, D.; Vazquez-Sanchez, S.; Tapia, O.; Toprani, D.; Beccari, M. S.; Yates, J. R., 3rd; Da Cruz, S.; Newby, J. M.; Lafarga, M.; Gladfelter, A. S.; Villa, E.; Cleveland, D. W. HSP70 chaperones RNA-free TDP-43 into anisotropic intranuclear liquid spherical shells. *Science* **2021**, *371*, No. eabb4309.
(53) Reinkemeier, C. D.; Lemke, E. A. Synthetic biomolecular condensates to engineer eukaryotic cells. *Curr. Opin. Chem. Biol.* **2021**, *64*, 174−181.
(54) Lasker, K.; Boeynaems, S.; Lam, V.; Stainton, E.; Jacquemyn, M.; Daelemans, D.; Villa, E.; Holehouse, A. S.; Gitler, A. D.; Shapiro, L. A modular platform for engineering function of natural and synthetic biomolecular condensates. **2021**, bioRxiv 2021.02.03.429226.
(55) Boeynaems, S.; Dorone, Y.; Marian, A.; Shabardina, V.; Huang, G.; Kim, G.; Sanyal, A.; Şen, N.-E.; Docampo, R.; Ruiz-Trillo, I.; Lasker, K.; Auburger, G.; Kabashi, E.; Gitler, A. D. Poly(A)-binding protein is an ataxin-2 chaperone that emulsifies biomolecular condensates. **2021**, bioRxiv 2021.08.23.457426.
(56) Yoshikawa, M.; Yoshii, T.; Ikuta, M.; Tsukiji, S. Synthetic Protein Condensates That Inducibly Recruit and Release Protein Activity in Living Cells. *J. Am. Chem. Soc.* **2021**, *143*, 6434−6446.
(57) Boyd, J. D.; Lee-Armandt, J. P.; Feiler, M. S.; Zaarur, N.; Liu, M.; Kraemer, B.; Concannon, J. B.; Ebata, A.; Wolozin, B.; Glicksman, M. A. A high-content screen identifies novel compounds that inhibit stress-induced TDP-43 cellular aggregation and associated cytotoxicity. *J. Biomol. Screen* **2014**, *19*, 44−56.
(58) Jackrel, M. E.; Shorter, J. Potentiated Hsp104 variants suppress toxicity of diverse neurodegenerative disease-linked proteins. *Dis. Models Mech.* **2014**, *7*, 1175−1184.
(59) Elden, A. C.; Kim, H.-J.; Hart, M. P.; Chen-Plotkin, A. S.; Johnson, B. S.; Fang, X.; Armakola, M.; Geser, F.; Greene, R.; Lu, M. M.; Padmanabhan, A.; Clay-Falcone, D.; McCluskey, L.; Elman, L.; Juhr, D.; Gruber, P. J.; Rüb, U.; Auburger, G.; Trojanowski, J. Q.; Lee, V. M.-Y.; Van Deerlin, V. M.; Bonini, N. M.; Gitler, A. D. Ataxin-2 intermediate-length polyglutamine expansions are associated with increased risk for ALS. *Nature* **2010**, *466*, 1069−1075.
(60) Peggion, C.; Massimino, M. L.; Stella, R.; Bortolotto, R.; Agostini, J.; Maldi, A.; Sartori, G.; Tonello, F.; Bertoli, A.; Lopreiato, R. Nucleolin Rescues TDP-43 Toxicity in Yeast and Human Cell Models. *Front. Cell. Neurosci.* **2021**, *15*, 625665.
(61) Frost, N. A.; Shroff, H.; Kong, H.; Betzig, E.; Blanpied, T. A. Single-molecule discrimination of discrete perisynaptic and distributed sites of actin filament assembly within dendritic spines. *Neuron* **2010**, *67*, 86−99.
(62) Fischer, J. W.; Busa, V. F.; Shao, Y.; Leung, A. K. L. Structure-Mediated RNA Decay by UPF1 and G3BP1. *Mol. Cell* **2020**, *78*, 70−84.
(63) Thayer, J. A.; Awad, O.; Hegdekar, N.; Sarkar, C.; Tesfay, H.; Burt, C.; Zeng, X.; Feldman, R. A.; Lipinski, M. M. The PARK10 gene USP24 is a negative regulator of autophagy and ULK1 protein stability. *Autophagy* **2020**, *16*, 140−153.
(64) Schindelin, J.; Arganda-Carreras, I.; Frise, E.; Kaynig, V.; Longair, M.; Pietzsch, T.; Preibisch, S.; Rueden, C.; Saalfeld, S.; Schmid, B.; Tinevez, J.-Y.; White, D. J.; Hartenstein, V.; Eliceiri, K.; Tomancak, P.; Cardona, A. Fiji: an open-source platform for biological-image analysis. *Nat. Methods* **2012**, *9*, 676−682.
(65) Ollion, J.; Cochennec, J.; Loll, F.; Escudé, C.; Boudier, T. TANGO: a generic tool for high-throughput 3D image analysis for studying nuclear organization. *Bioinformatics* **2013**, *29*, 1840−1841.
(66) Jumper, J.; Evans, R.; Pritzel, A.; Green, T.; Figurnov, M.; Ronneberger, O.; Tunyasuvunakool, K.; Bates, R.; Žídek, A.; Potapenko, A.; Bridgland, A.; Meyer, C.; Kohl, S. A. A.; Ballard, A. J.; Cowie, A.; Romera-Paredes, B.; Nikolov, S.; Jain, R.; Adler, J.; Back, T.; Petersen, S.; Reiman, D.; Clancy, E.; Zielinski, M.; Steinegger, M.; Pacholska, M.; Berghammer, T.; Bodenstein, S.; Silver, D.; Vinyals, O.; Senior, A. W.; Kavukcuoglu, K.; Kohli, P.; Hassabis, D. Highly accurate protein structure prediction with AlphaFold. *Nature* **2021**, *596*, 583−589.
(67) Varadi, M.; Anyango, S.; Deshpande, M.; Nair, S.; Natassia, C.; Yordanova, G.; Yuan, D.; Stroe, O.; Wood, G.; Laydon, A.; Žídek, A.; Green, T.; Tunyasuvunakool, K.; Petersen, S.; Jumper, J.; Clancy, E.; Green, R.; Vora, A.; Lutfi, M.; Figurnov, M.; Cowie, A.; Hobbs, N.; Kohli, P.; Kleywegt, G.; Birney, E.; Hassabis, D.; Velankar, S. AlphaFold Protein Structure Database: massively expanding the structural coverage of protein-sequence space with high-accuracy models. *Nucleic Acids Res.* **2022**, *50*, D439−d444.
(68) Ludwiczak, J.; Winski, A.; Szczepaniak, K.; Alva, V.; Dunin-Horkawicz, S. DeepCoil-a fast and accurate prediction of coiled-coil domains in protein sequences. *Bioinformatics* **2019**, *35*, 2790−2795.

https://doi.org/10.1021/acschemneuro.2c00156
ACS Chem. Neurosci. XXXX, XXX, XXX−XXX

Supporting Information

Sequestration of TDP-43$^{216-414}$ aggregates by cytoplasmic expression of the proSAAS chaperone

Juan R. Peinado[1,2#], Kriti Chaplot[2#], Timothy S. Jarvela[2],

Edward M. Barbieri[3], James Shorter[3] and Iris Lindberg[2*]

#Co-first authors

[2:] Department of Anatomy and Neurobiology, University of Maryland School of Medicine, University of Maryland, Baltimore, MD 21201 USA

[3.] Department of Biochemistry and Biophysics, Perelman School of Medicine, University of Pennsylvania, Philadelphia, PA 19104, USA

[1:] Present address: Department of Medical Sciences, Ciudad Real Medical School, Oxidative Stress and Neurodegeneration Group, Regional Center for Biomedical Research, University of Castilla-La Mancha (UCLM), Ciudad Real, Spain

* Correspondence should be addressed to: Iris Lindberg, Ph.D.

Email: ilindberg@som.umaryland.edu

Supporting Information

Supplemental Figure S1. Cyto-proSAAS forms spheres in various cell types, serving as a potential platform to identify encapsulated cytoplasmic targets.

Panel A: Representative confocal images of Neuro2A cells transfected with cyto-proSAAS cDNA for either 24 h (*left*) or 48 h (*right*) showing characteristic Flag-immunoreactive spheres (shown enlarged at right). **Panel B:** Overexpressed cyto-proSAAS forms spheres that can be observed using phase-contrast microscopy (*left side*, **yellow arrows**) and which consists of mostly unprocessed 30 kDa proSAAS, observed as a band in a Western blot using FLAG antibody (*right side*). **Panel C:** Expression of cyto-proSAAS in primary rat hippocampal cells results in the formation of spheres similar to those observed in Neuro2A and HEK cells. The border of the transfected cell is outlined in white. **Panel D:** Expression of Cherry-cyto-proSAAS (*red*) generates dispersed cytosolic aggregates in Neuro2A cells. **Panel E:** Representative images of GFP-tagged Tau; Tau E14; α-synuclein; α-synuclein A53T; TDP-$43^{216-414}$; HTT-Q74; and HA-tagged HTT-Q74. Images were taken at 40X at 24h after transfection. Scale bar, 10 μm. Magnified inserts correspond to 10 μm.

Figure S1

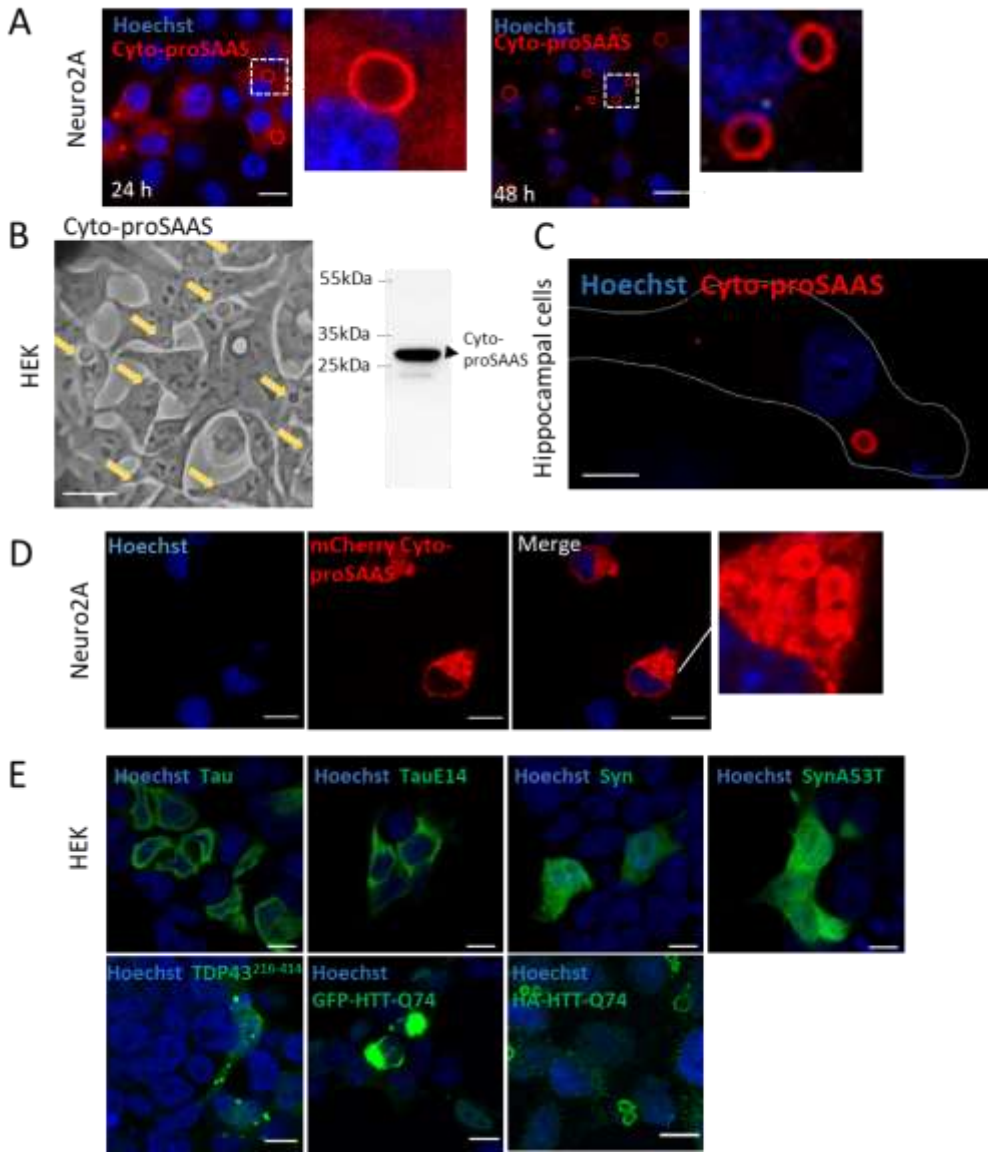

Supplemental Figure S2. Cyto-proSAAS spheres specifically encapsulate TDP-43$^{216-414}$ aggregates, but not HTT-Q74.
Panel A Cyto-proSAAS expression alone. **Panel B:** TDP-43$^{216-414}$ aggregates**,** but not HTT-Q74 aggregates (**panel C**) nor GFP-HTT-Q74 aggregates **(panel D)** are found inside cyto-proSAAS spheres (*red*) in HEK cells. **Panel E** shows the characteristic cytosolic fluorescence of dispersed mCherry (*red*) aggregates that never become accumulated within cyto-proSAAS spheres (*green*). Images were taken at 40X 24 h after transfection. Scale bar, 10 μm. Magnified images correspond to 10 μm.

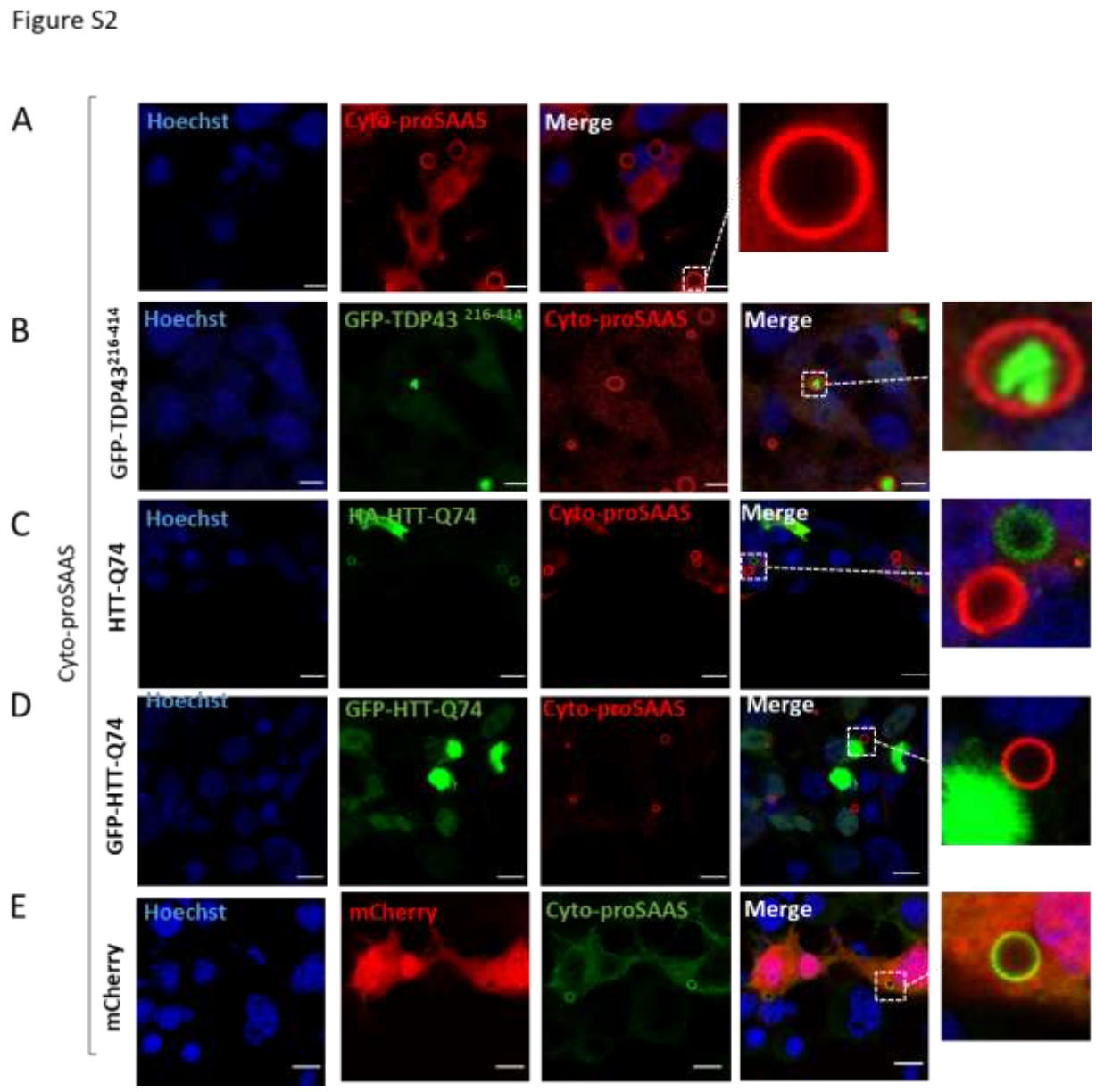

Supporting Information

Supplementary Movie 1. Dynamic imaging of mCherry-cyto-proSAAS spheres showing fusion of large spheres. Dynamic widefield microscopy of mCherry-cyto-proSAAS (*red*), beginning 18 h post transfection of cyto-proSAAS and mCherry-cyto-proSAAS (1: 0.2 ratio). The movie is 17 h long, with images taken every 2 min.

Supplemental Movie 2. Dynamic imaging of mCherry-cyto-proSAAS spheres showing sphere fusion with simultaneous GFP-TDP-43$^{216-414}$ sequestration.
Movie of **Figure 2D**. Dynamic widefield microscopy of mCherry-cyto-proSAAS *(red*) and GFP-TDP-43$^{216-414}$ (*green*), and DIC (*grayscale*) beginning 18 h post transfection of cyto-proSAAS, GFP-TDP-43$^{216-414}$ and mCherry-cyto-proSAAS (1:1:0.2 ratio). Each frame corresponds to 2 min in real time, and the length of the movie is 4 h and 45 min. The ImageJ plugin Linear Stack Alignment with SIFT was used to stabilize the movie around the transfected cell.

Supplemental Figure S3. Cyto-proSAAS spheres are not associated with cellular markers of autophagy, lysosomes, Golgi, lipid droplets, cell stress, and stress granules.

Panel A: No fluorescent signal was observed associated with cyto-proSAAS spheres following triple transfection of LC3-Cherry, cyto-proSAAS and GFP-TDP-43$^{216-414}$ cDNAs.

Panels B-D: Lack of cyto-proSAAS sphere immunostaining with antiserum against Lamp-1 (**panel B**); with Lysotracker (**panel C**); with anti-giantin antiserum (**panel D**); and with Bodipy (**panel E**). Arrows indicate cyto-proSAAS spheres.

Panels E-F: Cyto-proSAAS neither associates with HSP70 nor sequesters the co-expressed stress granule marker GFP-G3BP1. Scale bar, 10 μm.

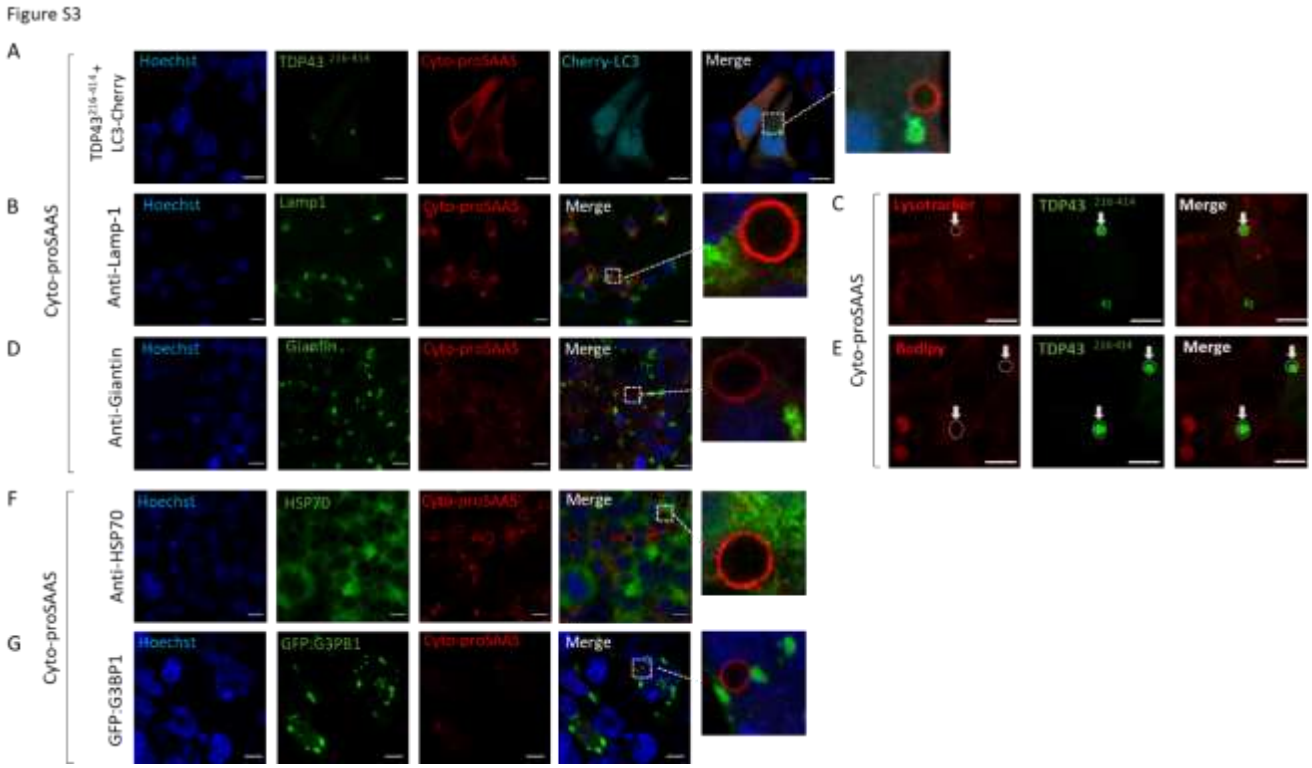

Supplemental Figure S4. Co-expression of cyto-proSAAS increases the cellular half-life of GFP-TDP-43$^{216-414}$.
Panel A: HEK cells transfected with cDNAs encoding GFP-TDP-43$^{216-414}$ alone, or in combination with cyto-proSAAS, were monitored by Western blotting using an anti-GFP antibody (*left panels*). Quantitation of triplicates is shown in below the blot. Approximately 80% of GFP-TDP-43$^{216-414}$ disappears after 6 h of cycloheximide treatment when cells are co-transfected with an empty vector; however, 43% remains in cells co-transfected with cyto-proSAAS cDNA (*, p<0.05).
Panel B: Confocal images taken prior to and following cycloheximide treatment confirm reduced cellular quantities of GFP-TDP-43$^{216-414}$ following cycloheximide treatment in the absence of cyto-proSAAS expression (*left panels*); in contrast, TDP-43$^{216-414}$ fluorescence is retained within cyto-proSAAS spheres (*right panels*). Scale bar, 10 μm.
Panels C-E: Ratio of the total surface area of GFP-TDP-43$^{214-416}$ to the total volume of the same objects (**C**); the mean pixel intensity for each group (**D**); and the total signal intensity of each group (**E**), determined by the sum of signal intensity of all pixels in that group. (n=12 cells, two-tailed paired t-test **p<0.05, **p<0.01, ***p<0.001*).

Figure S4

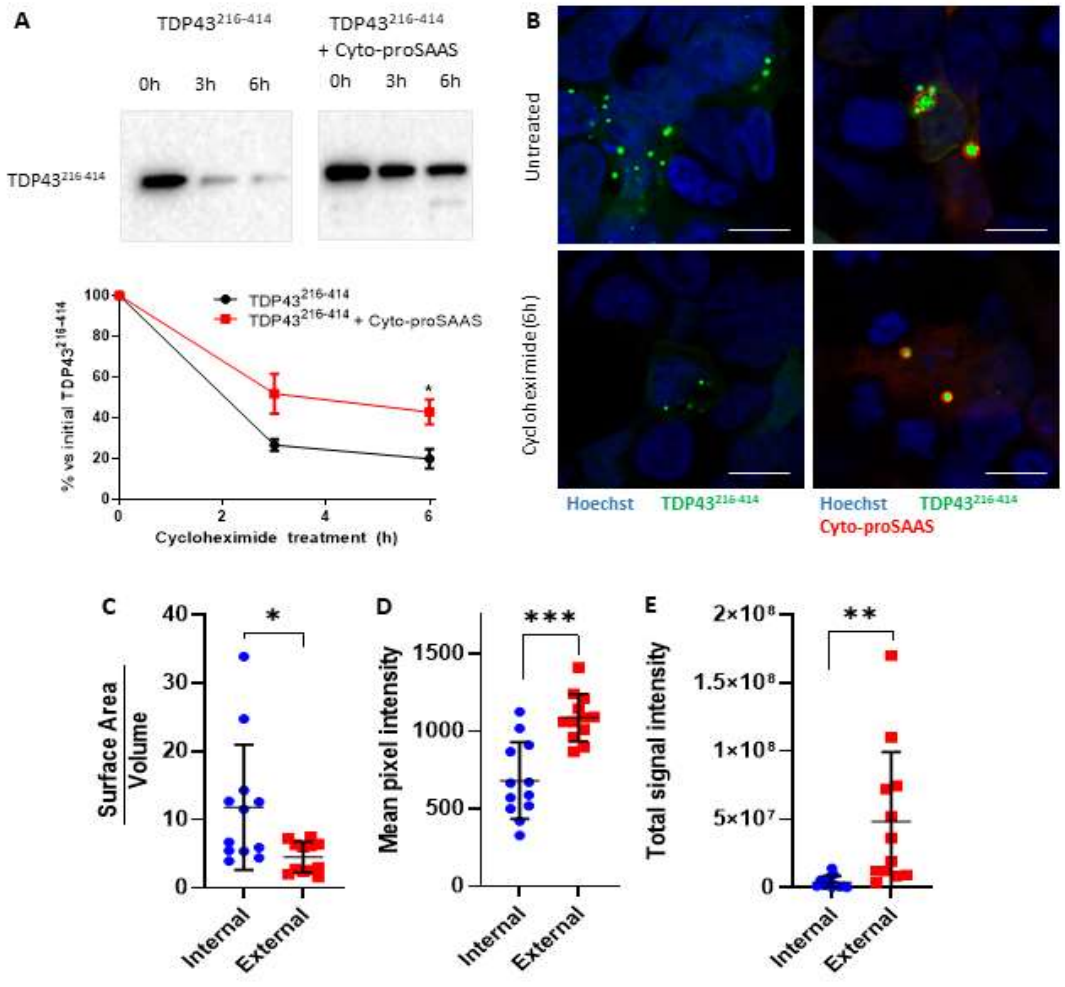

Supporting Information

Supplemental Figure S5: Cyto-proSAAS does not encapsulate N-terminal fragments of TDP-43, A. GFP-TDP-43$^{1-274}$ or B. GFP-TDP-43$^{1-193}$. Scale bar, 10 μm.

Figure S5

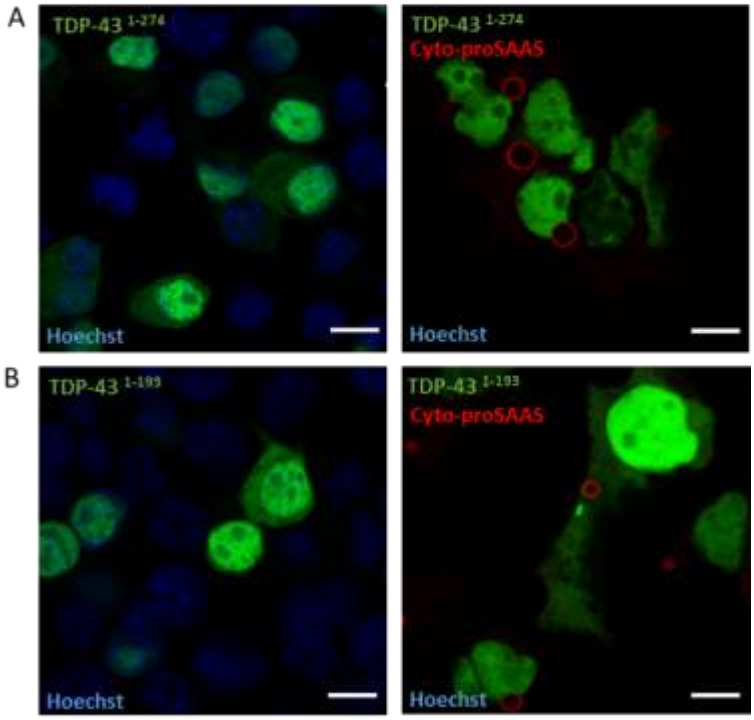

Supporting Information

Supplemental Figure S6: ProSAAS contains intrinsically disordered domains and low complexity regions.

ProSAAS domains (**Panel A**) containing overlapping low complexity regions (LCRs) (**Panel B**) and intrinsically disordered domains (IDDs) (**Panel C**) as predicted by SEG (PlaToLoCo) and PONDR bioinformatics tools, respectively. **Panel A** also shows the highlighted coiled coil region spanning the sequence from 32-80 amino acids.

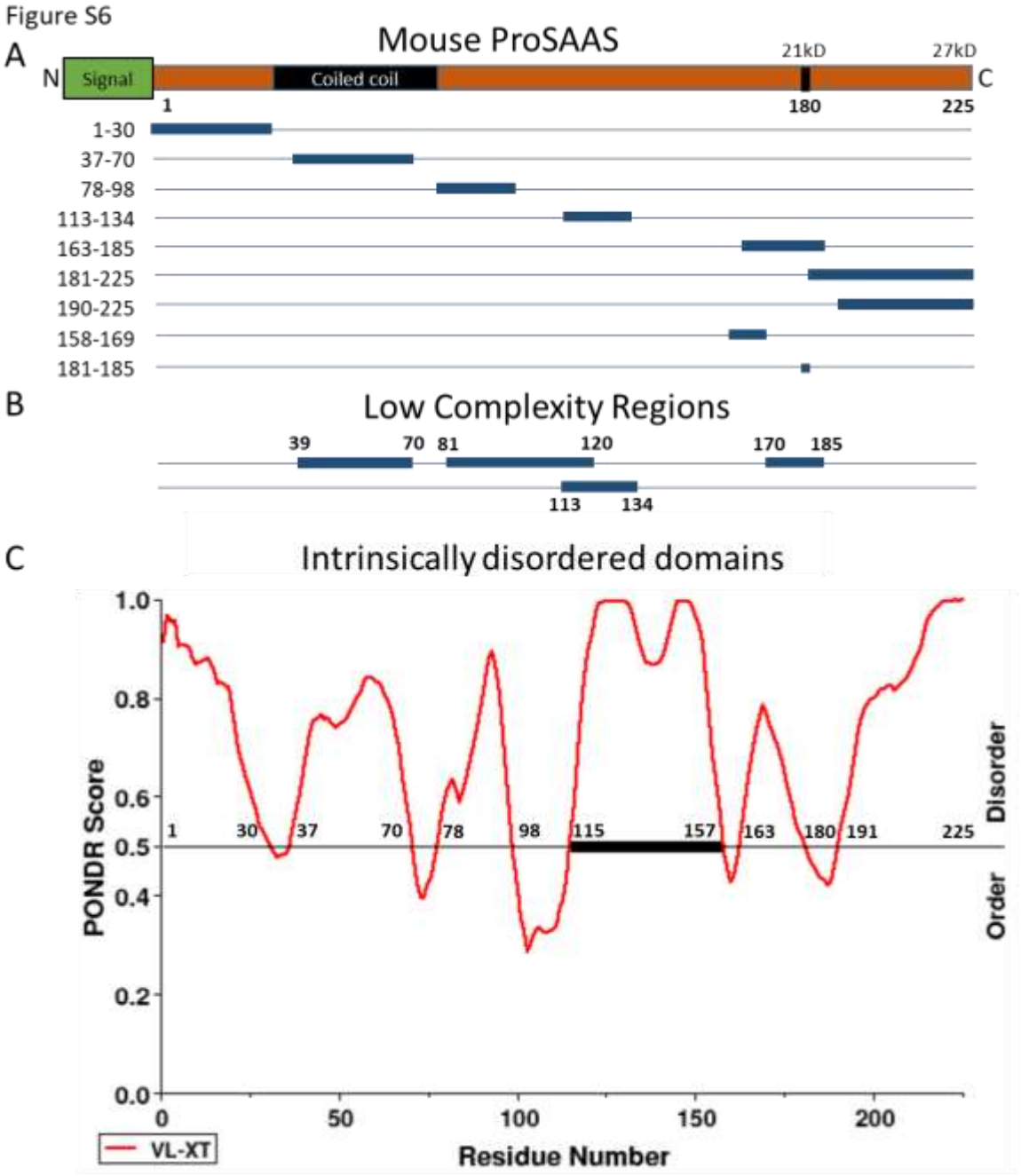

Supporting Information

Supplemental Figure S7: Affinity purification of His-tagged TDP-43-MBP and 27 kDa proSAAS
Panel A: TDP-43-MBP was purified using a two-step affinity chromatography procedure. Clarified bacterial lysate was first purified by Ni/NTA chromatography and pooled eluates were further purified on an amylose resin-containing column. Eluates 1-3 containing TDP-43-MBP protein (~89 kDa) were pooled and concentrated using 50 kDa spin columns before being aliquoted and frozen at -80°C until use.
Panel B: ProSAAS purification- Clarified lysate was purified by Ni/NTA chromatography and fractions 7-11 containing 27 kDa His-tagged proSAAS were pooled and dialyzed first against 100 mM acetic acid and then into 5 mM acetic acid. Samples were then aliquoted and stored at -80°C until use.

Figure S7